Double hypernuclei with nuclear-emulsion detector

Aung Nay Lin Nyaw

1183915001

A DISSERTATION

SUBMITTED TO THE ENVIROMENTAL AND RENEWABLE

ENERGY SYSTEM DIVISION,

GRADUATE SCHOOL OF ENGINEERING,

GIFU UNIVERSITY

March, 2021

Abstract

An experimental analysis of double hypernuclei (DH) with two units of strangeness such as double-Λ hypernuclei (DLH) or Ξ hypernuclei (XH) was performed with nuclear emulsion technologies. For DH measurement, Ξ^- hyperons were produced via the reaction of $K^- + p \rightarrow K^+ + \Xi^-$ by irradiating 1.13×10^{11} K^- meson beams with the momentum of 1.8 GeV/c on the diamond target at J-PARC K1.8 beam line. In total, ~10^4 Ξ^- hyperons were estimated to be stopped in 118 stacks of emulsion sheets. By following of Ξ^- tracks in the emulsion layers for 2 years, 33 DH events were detected. Among these, a DLH event was named D001 and two XH events were named IBUKI and IRRAWADDY. The reaction process, $\Xi^- + {}^{14}\mathrm{N} \rightarrow {}^{10}_{\Lambda\Lambda}\mathrm{Be} + {}^{4}\mathrm{He} + \mathrm{n}$, was interpreted as the most likely case of D001 event. The binding energy ($B_{\Lambda\Lambda}$) between two Λ hyperons and the core nucleus, and the interaction strength ($\Delta B_{\Lambda\Lambda}$) of the two Λ hyperons with each other for ${}^{10}_{\Lambda\Lambda}\mathrm{Be}$ were obtained to be 15.22 ± 2.77 MeV and 1.80 ± 2.77 MeV, respectively. This $\Delta B_{\Lambda\Lambda}$ reveals a weakly attraction. The IBUKI event was uniquely identified as Ξ^- + ^{14}N bound system with the reaction process of $\Xi^- + {}^{14}\mathrm{N} \rightarrow {}^{10}_{\Lambda\Lambda}\mathrm{Be} + {}^{5}_{\Lambda}\mathrm{He}$. The IRRAWADDY event was also uniquely identified as Ξ^- + ^{14}N bound system with the reaction of $\Xi^- + {}^{14}\mathrm{N} \rightarrow {}^{5}_{\Lambda}\mathrm{He} + {}^{5}_{\Lambda}\mathrm{He} + {}^{4}\mathrm{He} + \mathrm{n}$. The binding energy, B_{Ξ^-}, of Ξ^- + ^{14}N system (${}^{15}_{\Xi}\mathrm{C}$), of these XH events were measured to be 1.27 ± 0.21 MeV and 6.27 ± 0.27 MeV, respectively. In considering the experimental data and theoretical calculation, the energy levels of Ξ^- of IBUKI and IRRAWADDY events will be the experimental evidences, for the first time, of the nuclear 1*p* and 1*s* states of ${}^{15}_{\Xi}\mathrm{C}$, respectively.

Contents

Chapter 1

Introduction

1.1 Nuclear and hypernuclear physics

In particle physics, there are six kinds of fundamental quarks namely up (u), down (d), strange (s), and charm (c), bottom (b), top (t) quarks. Among these quarks, u-, d-, and s-quarks are light quarks. The baryon group particles are made up of three quarks out of the six quarks. It can be divided into two sub-group called: (i) Nucleon (N) (proton (uud) and/or neutron (udd)) which is composed up without s-quark, and (ii) Hyperon (Y) {lambda (Λ), sigma (Σ), Xi (Ξ), omega (Ω)} which are composed up with at least one s-quark. The quarks composition of hyperons is: Λ^0 (uds), Σ^+ (uus), Σ^0 (uds), Σ^- (dds), Ξ^0 (uss), Ξ^- (dss), and Ω^- (sss) respectively.

Protons (p) and neutron (n), consist of only u- and d- quarks, and they have almost the same properties except for their charge. Thus, a proton and a neutron can be considered to be identical particles that differ only in the *z*-component of isospin. They are described by isospin vectors which are orthogonal to each other. That is, nucleons are expressed in the isospin 2-dimensional special unitary group SU (2). The N-N interaction could be understood under the isospin SU (2) symmetry. Assuming the masses of u, d and s quarks are the same, they can be considered as the identical particles except for the difference in the quantum number of flavors. A baryon consisting of these quarks is expressed by flavor 3-dimensional special unitary group SU (3).

Nucleus is a positive charged core of the atom and every matter are made up by composing of atoms. Normal nucleus is made up of nucleons via the strong interaction. Hypernucleus is made up of baryon including at least one hyperon via the strong interaction. Understanding the strong interaction leads to understanding the formation and the diversity of matter.

Nucleons and hyperons, are classified into the octet with spin 1/2 and the decuplet with spin 3/2. The baryon octet is represented using the axes for isospin (I_3) and for strangeness (S) as shown in figure 1.1. Protons and neutrons are classified as S = 0 had been investigated by numerous scattering experiments. On the other hand, scattering experiments with the hyperons are difficult due to their short lifetime of the order of 100 ps. Researches on the S = −1 systems, such as Λ hypernuclei and Σ hypernuclei, have progressed at KEK, BNL, J-PARC, JLab and MAMI. In particular, spectroscopy of Λ hypernuclei has been well studied as reviewed in [1]. Information

* “s” represented the strange-quark. ** “S” represented the strangeness of the quark.

on the ΛN interaction has been obtained from such experimental researches together with theoretical studies. Σ-hypernuclear state was searched for by the reaction spectroscopy experiment at KEK- PS via the (π^-, K^+) reaction and it was found that the Σ^- N interaction was repulsive [2]. On the other hand, for the ΞN interaction, the experimental data are especially limited.

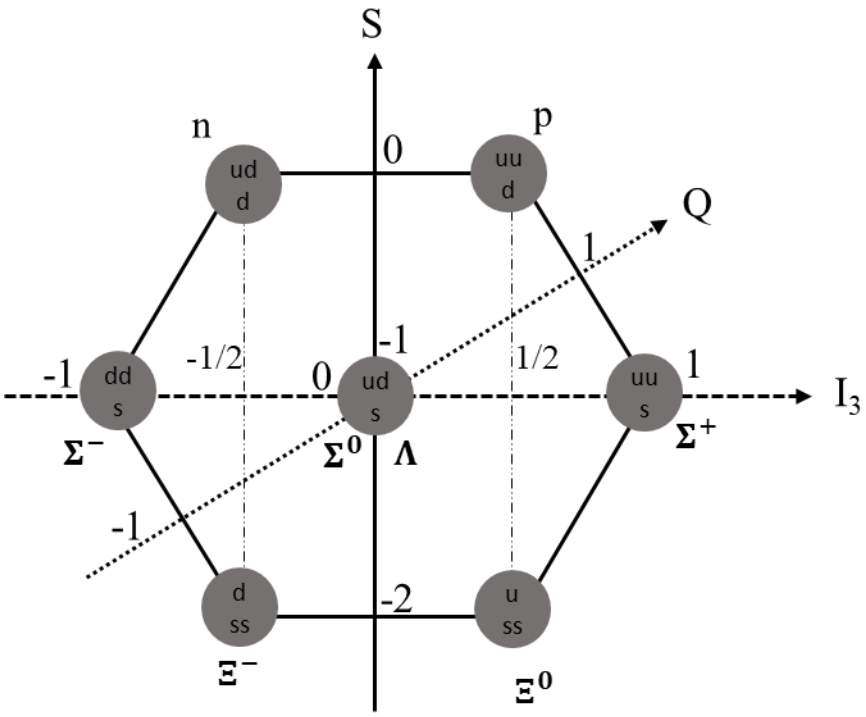

Fig 1.1. The baryon octet with spin-parity $1/2^+$. The solid vertical line is the strangeness, the rectangle-dotted horizontal line represents the isospin, and the star-dotted inclined line represents the charge of particles.

1.2 Motivation on S = − 2 system

Ξ^- particle, one of the hyperons, contains two s-quarks and occupies the mass of 1321.71 ± 0.07 MeV/c^2 and lifetime of 163.9 ± 0.015 ps [3]. For S = -1 sector, the Y-N interaction could be investigated to understand the baryon-baryon interactions under the flavor SU (3) symmetry such as ΛN and ΣN interactions. For the S = −2 sector, there is a difficulty in order to performed the S = − 2 system with Ξ^- and Ξ^- hyperons due the small cross section of Ξ production. For this reason, experimental studies on S = −2 system such as Ξ^- hypernuclei and/ or double-Λ hypernuclei are extremely limited so far even though they are essential for the general understanding of the baryon-baryon interaction.

From many theoretical estimated results, Y-N interaction plays in the important role for understanding neutron stars. A neutron star, small size and dense star < $1/10^6$ times radius and ~2 times dense of that of the sun, is produced after a supernova explosion. It is mainly composed with neutron. In such high-density matter, some neutrons occupy high-lying orbits because they cannot occupy the same orbit with others due to the Pauli's exclusion principle. In such situation, to reduce a fermi energy, some of the neutrons are expected to convert to other particles which are not affected by the Pauli's principle and Λ and Ξ^- hyperons are the candidates [3]. Thus, studying of Y-N and Y-Y interactions give us information about the hyperons in neutron stars. Since the neutron star could not be investigate experimentally, the emulsion experiments were performed.

1.3. S = −2 hypernuclei

Nuclear emulsion has been used for various experiments to detect a sequential weak decay of hypernuclei in the S = −2 sector. The Ξ^- hyperons are produced in the quasi-free reaction, $K^- + p \rightarrow \Xi^- + K^+$, were studied in the emulsion. Especially, the postulate of Ξ^- hyperons captured at rest by the emulsion and Ξ^- hypernucleus is produced. Then, Ξ^- decays into two Λ hyperons via the reaction; $\Xi^- + p \rightarrow \Lambda + \Lambda + 28$ MeV and double-Λ hypernucleus, twin single-Λ hypernuclei, or single-Λ hypernuclei could be produced.

Several emulsion experiments reported the production of double-Λ hypernuclei and twin single-Λ hypernuclei, where two single-Λ hypernuclei were produced simultaneously after the formation of a Ξ^- hypernucleus or a Ξ^- atom.

1.3.1 Double-Λ hypernucleus

Double-Λ hypernuclei have been investigated to study the ΛΛ interaction. Mass of a double-Λ hypernucleus, $M\left({}^{A}_{\Lambda\Lambda}Z\right)$, is measured in an experiment and the binding energy, $B_{\Lambda\Lambda}\left({}^{A}_{\Lambda\Lambda}Z\right)$, is obtained as

$$B_{\Lambda\Lambda}\left({}^{A}_{\Lambda\Lambda}Z\right) = M\left({}^{A-2}Z\right) + 2M(\Lambda) - M\left({}^{A}_{\Lambda\Lambda}Z\right) \quad (1.1)$$

From that, the ΛΛ bonding energy is calculated as

$$\Delta B_{\Lambda\Lambda}\left({}^{A}_{\Lambda\Lambda}Z\right) = B_{\Lambda\Lambda}\left({}^{A}_{\Lambda\Lambda}Z\right) - 2B_{\Lambda}\left({}^{A-1}_{\Lambda}Z\right) \quad (1.2)$$

where B_Λ represent the binding energies of a Λ hyperon in a single hypernucleus. The $\Delta B_{\Lambda\Lambda}$ indicates the binding energy between the two Λ hyperons by assuming that the binding energy of a Λ hyperon in a nucleus does not change from single-Λ hypernucleus.

Since the double-Λ hypernucleus has two Λ hyperons in a nucleus, it shows typical event pattern in the emulsion. The first double-Λ hypernucleus event was observed by Danysz in 1963 in an experiment at CERN [4] using the directly interaction of K^- beam with a momentum of 1.5 GeV/c into the emulsion. This event was interpreted as the mesonic cascade decay of a double-Λ hypernucleus of ${}^{10}_{\Lambda\Lambda}$Be or ${}^{11}_{\Lambda\Lambda}$Be. The $\Delta B_{\Lambda\Lambda}$ values were obtained to be 4.5 ± 0.4 MeV and 3.2 ± 0.6MeV for ${}^{10}_{\Lambda\Lambda}$Be and ${}^{11}_{\Lambda\Lambda}$Be, respectively.

The KEK-PS E176 counter-emulsion hybrid experiment [5] was adopted for the first time to observe double-Λ hypernuclei. Track of Ξ^- hyperon in the emulsion was traced from the reaction vertex which was detected by tracing K^+ meson from the downstream. Emulsion sheets with a changeable sheet (CS) which was located at the downstream side were irradiated by 1.66 GeV/c K^- beam. Among 98 candidates of Ξ^- stopping events, four events showed the sequential weak decay topology. One event (#15-03-37) was identified as the production and decay of ${}^{10}_{\Lambda\Lambda}$Be or ${}^{13}_{\Lambda\Lambda}$B [6]. The $B_{\Lambda\Lambda}$ values for each mode were obtained to be 8.5 ± 0.7MeV and 27.6 ± 0.7MeV, respectively.

From the KEK-PS E373 experiment, the most impressive results were obtained from the event called NAGARA [7, 8] as shown in figure 1.2 (a) among all of the detected seven double-Λ hypernuclear events from 700 Ξ^- stopping cases. A counter-emulsion hybrid method with scintillating-fiber detectors was adopted to observe double-Λ hypernuclei efficiently. It was uniquely identified as ${}^{6}_{\Lambda\Lambda}$He. From the NAGARA events, the $B_{\Lambda\Lambda}$ and $\Delta B_{\Lambda\Lambda}$ were measured to be 6.91 ± 0.16 MeV and 0.67 ± 0.17 MeV, respectively [8]. ΛΛ interaction, especially its s-wave (${}^1S_0$) interaction, is found to be weakly attractive. This event became a standard to evaluate the Λ-Λ interaction.

Stimulated from this result, the current detected double-Λ hypernuclear events including the MINO event as presented by figure 1.2 (b) are examined. The MINO event was interpreted as one of the following three candidates [9]:

$$^{16}\mathrm{O} + \Xi^- \rightarrow ({}^{10}_{\Lambda\Lambda}\mathrm{Be}, {}^{11}_{\Lambda\Lambda}\mathrm{Be}, {}^{12}_{\Lambda\Lambda}\mathrm{Be}) + \left({}^{4}\mathrm{He}\right) + (\mathrm{t}, \mathrm{d}, \mathrm{p})$$

$B_{\Lambda\Lambda}$ ($\Delta B_{\Lambda\Lambda}$ of these double-Λ hypernuclei were obtained as 15.05 ± 0.11 MeV (1.63 ± 0.14 MeV), 19.07 ± 0.11 MeV (1.87 ± 0.37 MeV), and 13.68 ± 0.11 MeV (−2.7 ± 1.0MeV), respectively. The negative $\Delta B_{\Lambda\Lambda}$ value of ${}^{12}_{\Lambda\Lambda}$Be indicates that it was produced in the excited state. The most probable

interpretation was found to be the production and decay of the ${}^{11}_{\Lambda\Lambda}$Be nucleus from the kinematic fitting.

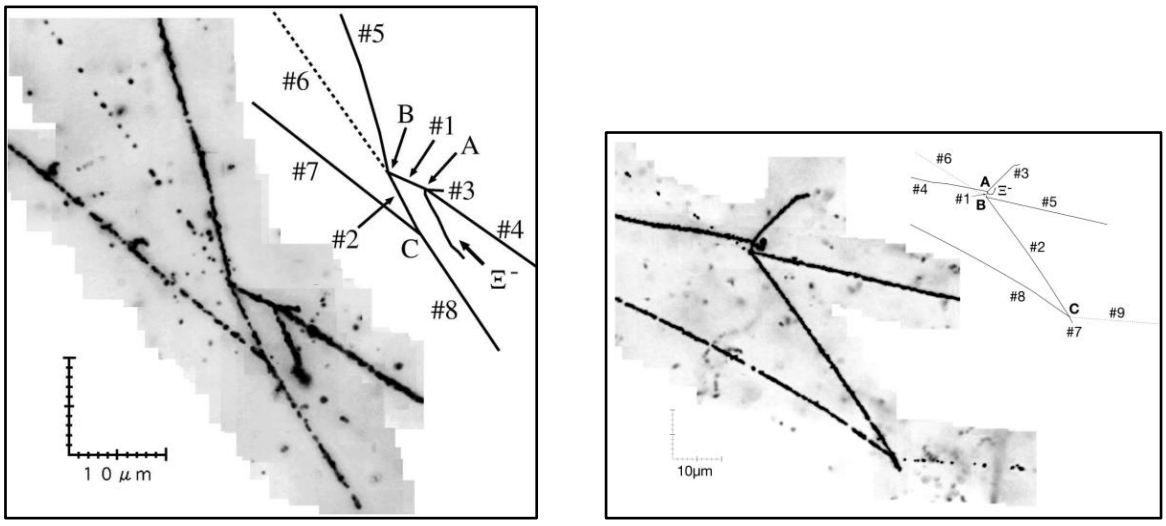

(a) (b)

Fig 1.2. (a) Superimposed image and schematics drawing of the NAGARA event detected in the previous KEK E373 experiment.

(b) Superimposed image and schematics drawing of the MINO event observed in the J-PARC E07 experiment.

ΛΛ s-wave interaction in ${}^{6}_{\Lambda\Lambda}$He from the uniquely identified NAGARA event was determined with good energy accuracy. However, the $\Delta B_{\Lambda\Lambda}$ value may change according to the change of core nucleus structure due to the existence of one more Λ. Moreover, other related interactions such as p-wave information of ΛΛ, ΛΛ-ΞN mixing are totally unknown. In particular, the ΛΛ-ΞN mixing is important on light s-shell double-Λ hypernuclei. In case of p-shell double-Λ hypernuclei, ΛΛ-ΞN mixing is suppressed due to the Pauli blocking because 1*s* orbits of nucleons are occupied. On the other hand, ΛΛ binding energy of s-shell double-Λ hypernuclei such as ${}^{4}_{\Lambda\Lambda}$H, ${}^{5}_{\Lambda\Lambda}$H, is considered to be sensitive to the ΛΛ-ΞN mixing.

Several theoretical groups calculated the structure of unobserved double-Λ hypernuclei and their results depend on the model [10-13]. Therefore, it is necessary to measure the ΛΛ binding energy in several double-Λ hypernucleus species systematically to guide the theoretical works.

1.3.2 Twin single-Λ hypernuclei

Information of the Ξ-N and Λ-Λ interaction has been extracted by measuring the binding energies of a Ξ^- hyperon and Λ hyperons in Ξ-hypernuclei and double-Λ hypernuclei, respectively. Since the electric charge of the Ξ^- hyperon is −1, Ξ^- hypernuclei have a different charge from the core nuclei. In hypernuclei, A and Z are defined as the baryon number and the electric charge, respectively. The Ξ^- hyperon in an atomic state of a nucleus may interact with the nucleus by the Ξ^- – nucleus interaction. Thus, the binding energy of the Ξ^- hyperon is defined as

$$B_{\Xi^-}\left({}^{A}_{\Xi}Z\right) = M\left({}^{A-1}Z + 1\right) + M(\Xi^-) - M\left({}^{A}_{\Xi}Z\right) \qquad (1.3)$$

where $B_{\Xi^-}\left({}^{A}_{\Xi}Z\right)$ is the binding energy of the Ξ^- hyperon in the Ξ^-- nucleus system. $M\left({}^{A-1}Z + 1\right)$, $M(\Xi^-)$, and $M\left({}^{A}_{\Xi}Z\right)$ are the masses of the core nucleus, the Ξ^- hyperon, and the Ξ^-- nucleus system, respectively.

Twin-Λ hypernuclei in emulsions are also an effective approach to study Ξ-hypernuclei. When Ξ^- is captured with a nucleus, two single-Λ hypernuclei are expected to be produced in a few % probability. These events can be identified with their decay topology. Since the mass of single-Λ hypernuclei are well known through the past measurements, the mass of initial state, Ξ^--nucleus system, can be estimated from the kinematics. The KISO event as shown in figure 1.3 is the first evidence of the deeply bound Ξ-hypernucleus system, Ξ^--^{14}N [14, 15]. This event was observed in the KEK-PS E373 experiment and ascribed to the following decay process:

$$^{14}\mathrm{N} + \Xi^- \rightarrow {}^{10}_{\Lambda}\mathrm{Be} + {}^{5}_{\Lambda}\mathrm{He}$$

with the Ξ^- binding energy (B_{Ξ^-}) of 1.03 ± 0.18 MeV or 3.87 ± 0.21 MeV. Since the state of daughter single-Λ hypernucleus ${}^{10}_{\Lambda}$Be was not uniquely identified, two interpretations are possible for the B_{Ξ^-} depending on the excitation energy of the ${}^{10}_{\Lambda}$Be. The experimental information of the Ξ-N and Λ-Λ interactions is quite essential to understand the baryon–baryon interaction.

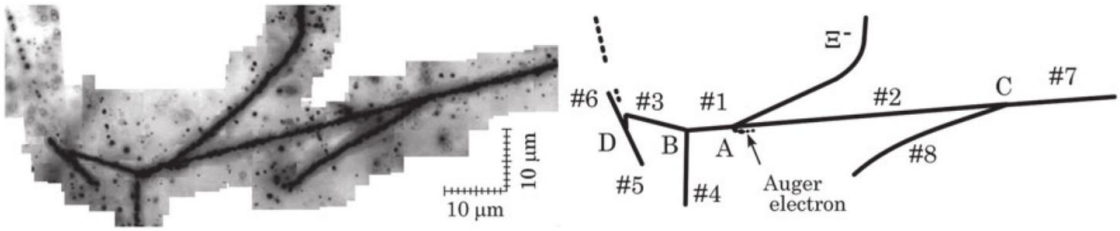

Fig 1.3. The superimposed image and its schematic drawing of the KISO event.

1.4 J-PARC E07

In the past experiment only a double-Λ hypernuclear event, NARAGA, and a twin hypernuclear event, KISO, show the impressive results of Λ-Λ interaction and Ξ^- hyperon binding energy with the core nucleus of Ξ^--^{14}N bound system. In order to determine the S = − 2 system clearly, it is necessary to detected a large amount of double hypernuclear event with uniquely identification of nuclide.

An experiment, J-PARC E07 was performed with an upgraded counter-emulsion hybrid experiment to accumulate 10 times as much data as that of E373 [16]. In E07, the emulsion volume and enhance the purity of K^- beam will be able increased. The emulsion scanning system was also developed from classical human eyes tracing to automatic microscope scanning system. Using the predicted set of Ξ^- position and angle obtained with silicon strip detectors (SSD), Ξ^- tracks in the emulsion could be automatically traced.

A mass production of nuclear emulsion plates of E07 were produced in 2013 and 2014, and beam exposure was carried out in 2016 and 2017. A total of 2.1 tons of emulsion was used. Emulsion scanning process was started from April, 2018. It was expected to detect 100 double hypernuclear events including new species among 1×10^4 Ξ^- stopping cases.

A newly detected double-Λ hypernuclear event, D001, and the most impressive new twin hypernuclear events in the world, IBUKI and IRRAWADDY, were interpreted and discussed in this paper.

Chapter 2

Experiment

2.1 Nuclear emulsion of J-PARC E07

Nuclear emulsion is a film like photographic plate manufactured by coding the emulsion, which contains the weight ratio of 50% of AgBr crystals and 50% of gelatin, on both sides of a polystyrene film (base) that serves as a support. E07 emulsion is the Fuji: NU-3GIFL type. The elements composition in the emulsion are described in Table 2.1. The size of AgBrI crystals was 0.2 μm in the Fuji: NU-3GIFL emulsion. It can record tracks of charged particles while passing through it with sub-μm spatial resolution, which is good enough to separate their weak decay vertices. In addition, the kinetic energies of these charged particles can be determined with $\Delta E/E \sim 1\%$ accuracy by their ranges. Therefore, the mass of double-Λ hypernuclei can be reconstructed with a good resolution, typically ~ 0.2MeV, by kinematic analysis of the production and decay modes.

The size of the E07 emulsion was set 35.0×34.5 cm^2 in area. Two type of emulsion plates are produced. (i) thin type plate with 100 μm emulsion layer on both sides of 180 μm Polystyrene film base and, (ii) thick type plate with 450 μm emulsion layers on the both sides of 40 μm Polystyrene film base. The base film is used for support to avoid separation of the emulsion during photographic development and to prevent wrinkles during stock for scanning. Thirteen plates are set as one emulsion stack (module) in the arrangement of two thin plate set as the first and last plates and the eleven thick type plates are sandwich in the middle as shown in figure 2.1. When the experiment was performed, they were installed in a special holder called the Emulsion Mover.

Table 2.1. Design value of the composition of the Fuji: NU-3GIFL emulsion.

Element	Density [g/cm^3]
H	0.05
C	0.326
N	0.11
O	0.23
Br	1.166
Ag	1.60
I	0.033
others	0.015

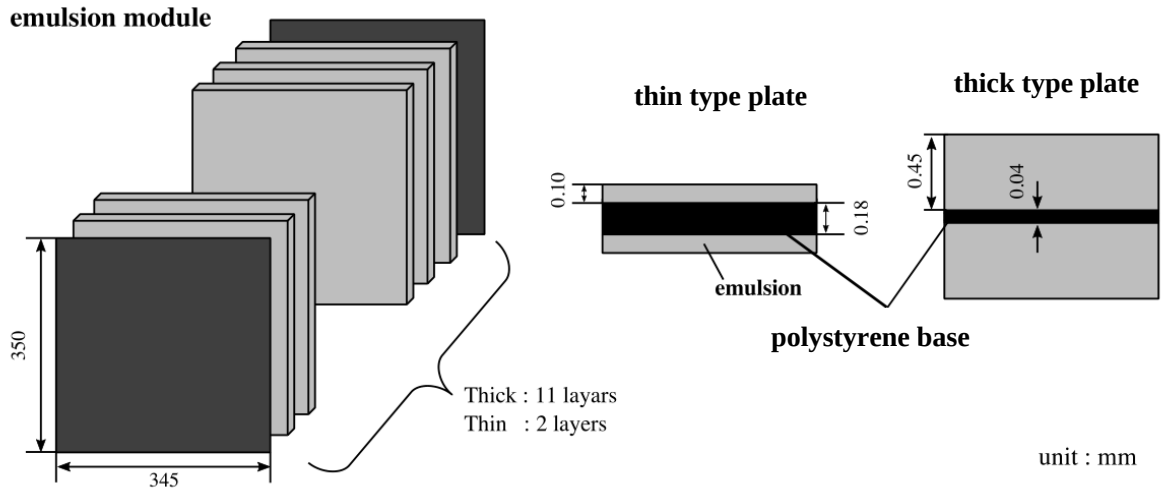

Fig 2.1: Emulsion sheet of E07 experiment.

2.2 Nuclear emulsion production

The nuclear emulsion of J-PARC E07 experiment was produced with a common hybrid-emulsion method as in the E373 experiment. Therefore, we prepared huge amount of emulsion gel of 2.1 tons, which is 3 times quantities of E373. The comparison of emulsion of E373 and E07 is descripted in Table 2.2 [16, 17].

Nuclear emulsion plates are produced with four steps, pouring, coating, drying and cutting, and it takes 11 days for one cycle. There are twelve cycles, two cycles for thin type plates and 10 cycles for thick type plates.

Table. 2.2 Experimental setup of E373 and E07

Track		KEK-E373	J-PARC E07
Beam Line		K2 beam	K1.8 beam
Beam Momentum		1.66 GeV/c	1.66 GeV/c
Ξ^- stop event		~10^3	~10^4
number of double hypernuclei		9	~100 (expected)
emulsion		Fuji ET-7C & ET-7D	Fuji GIF-003T
mass		800 kg	2100 kg
Ξ^- detector		SciFi-bundle	SSD
X-ray detector		-	Hyperball-X
Size ($cm^{2)}$		24.5×25.0	35.0×34.5
Thickness (μm)	thin plate	100+200+100	100+180+100
	thick plate	500+40+500	450+40+450

2.2 1 Emulsion pouring and drying

Before pouring the adhesion between base film and emulsion must be checked and improved because the emulsion can peel off from the base [18]. It is important to improve the hydrophilicity of the film by performing the treatment with gelatin or corona discharge. By passing the Base film between the insulated electrode and the dielectric roll and applying a high voltage to generate a corona discharge, gas components such as oxygen become a plasma state, and the

charged electrons are transferred to the resin surface. Drop a drop of water on the discharge-treated film and take a picture from the side with a camera and check the contact angle of a water drop and the film. The contact angle for the 40 μm base discharge treatment used in this production is expected to have 54.0 ˚ ± 0.8˚ necessarily and that for the 180 μm base at 57.3 ˚ ± 0.7˚ [18]. Figure 2.2 shows the hydrophilicity of the surface.

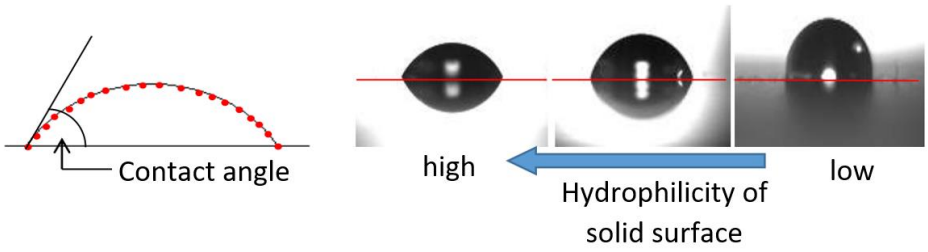

Fig 2.2: Schematic diagram of the contact angle (left). The pictures of water droplets taken with a camera (right) [18].

Another treatment method is pre-coating the base film with gelatin. Soak wash the film in the ion-exchange water to remove dust, dry for 2 to 3 hours, and then sets on stainless steel frame with vinyl tape. Coat the gelatin uniformly on the base film. The thickness of the 40 ± 0.9 μm base becomes 41.8 ± 0.6 μm and the 179.5 ± 1.0 μm base becomes 182.5 ± 0.8 μm.

After that, the emulsion is pouring by a pair of two people on one side of the cleaned base film. The base was set on the 71×70 cm^2 acrylic bars-mode which set on horizontal plane of the flat stone in order to get thickness accuracy of less than 5% as shown in figure 2.3. After drying the emulsion gel was set under 20°C for about 20 minutes, then dummy gel consisting of almost gelatin was poured around the emulsion to avoid its distortion at drying process. The emulsion sheets are set on the drying cabinet which has 10 cm spacing of drying space in each adjacent drying stage at the room temperature and humidity of 28 ± 1°C and 75 ± 5% respectively. Figure 2.4 shows the drying shelves. After two days' drying under this condition, surface coating was applied and set again in the drying cabinet for one day. At the final-dry process, the sheets were not placed on the drying rack, hanged in the drying room with the temperature at 25 ± 1°C and humidity 60 ± 5%. If the emulsion is not well dried (not too much dried), the plates stick by themselves very firmly and never been separated and image after beam exposure will be also faded. The emulsion layer on another side of base film was processed in the same manner as mentioned above.

(a)

(b)

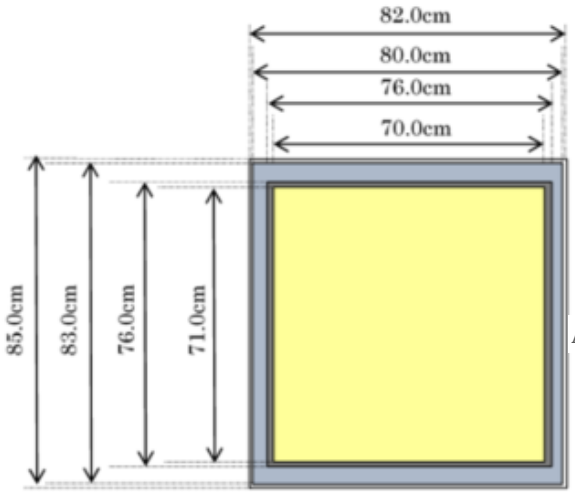

	Area 面積 [cm^2]
Acrylic board 板	85.0×82.0
Base	83.0×80.0
Emulsion	71.0×70.0
Dummy gel	76.0×76.0−(71.0×70.0)

(c)

Fig 2.3: (a) a stone surface plate used as an application table. (b) Applying the emulsion. (c) Size of the acrylic board, base film and emulsion [18].

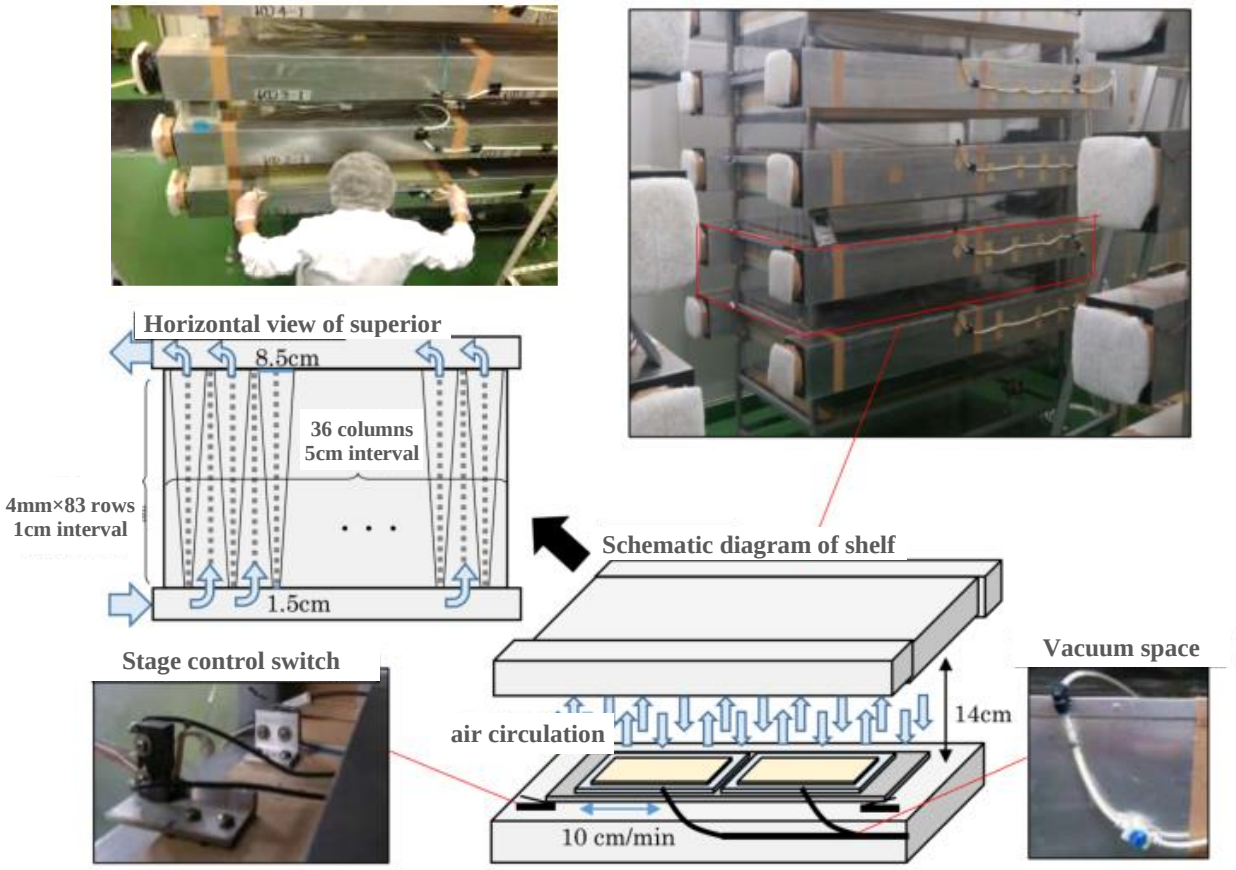

Fig 2.4 Drying shelves placed in the drying chamber. There are 6 shelves that can store 2 Emulsion sheets per unit. At the top of the shelf, air inlets and inlets are arranged alternately, and the air circulates at a uniform pressure everywhere. During drying, the stage on which the emulsion is placed is moved left and right by a motor to prevent local drying. A vacuum pump is placed on each drying rack to maintain the vacuum between the acrylic plate and Base [18].

2.2 2 Emulsion cutting

The produced dried-sheet (710 x 700 mm^2) was cut into 4 plates with the size of (350 x 345 mm^2) on the guillotine stage with the help of a metal bar for better accuracy of the plate size [18]. Figure 2.5 shows the schematic diagram of emulsion cutting. A maximum of 36 sheets (144 plates) can be produced in one cycle. Table. 2.3 shows the work schedule for one cycle. 11 days is needed to complete one cycle production. Total of 12 cycles production are performed in this way. Finally, 12 plates are assembled in each laminated bag sandwiched by glassine papers between the plates. The production period was 6 months long from December 2013 to May 2014, and totally 1360 thick type plate and 228 thin type plates were produced. Until the beam exposure time, the plates are kept in Kamioka mine in the lead box of 10 cm thick to avoid radiations, γ-rays and cosmic rays from the air. By this treatment, cosmic rays and also γ-rays via the Compton-electron checking were reduced by 90% rather than in environment.

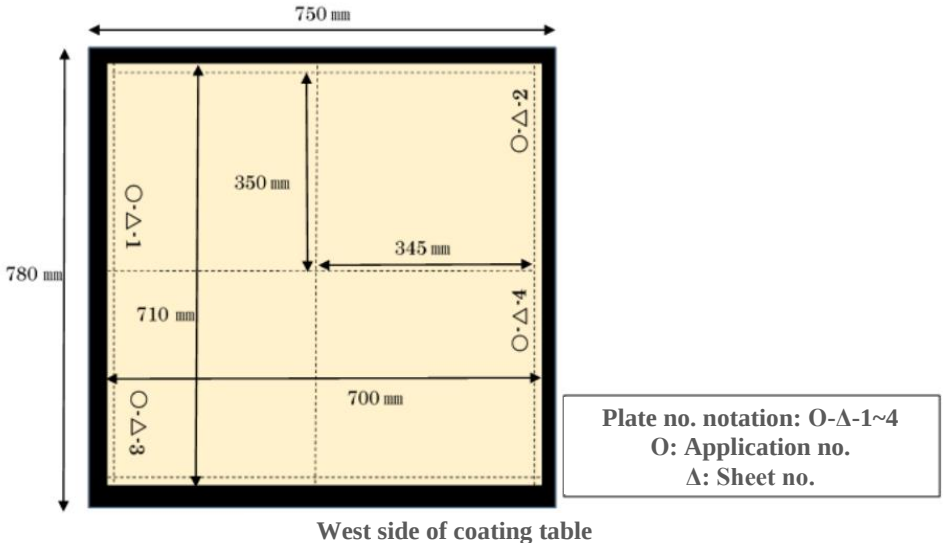

Fig 2.5: Schematic diagram of emulsion cutting [18].

Table 2.3 Schedule of the production of emulsion sheet in one cycle work [18].

schedule	Work process	
1st day	Room/equipment cleaning, emulsion/chemical preparation	
2nd day	Application 1st face	
3rd day		Application 1st face
4th day	Surface coat 1st face	
5th day		Surface coat 1st face
6th day	Application 2nd face	
7th day		Application 2nd face
8th day	Surface coat 2nd face	
9th day		Surface coat 2nd face
10th day	Final drying	
11th day	Cutting (36 big sheets → 144 plates)	

2.3 Beam exposure

The experiment was carried out using a 1.8 GeV/c K^- beam at the K1.8 beam line of the Hadron Experimental Facility at J-PARC [17, 18]. This beam line was designed to conduct S = −2 physics with the (K^-, K^+) reaction with high intensity and large K^-/π^- ratio. The beam intensity and purity were 2.8×10^5 kaons per spill (2s duration) and 82%, respectively. In order to measure momenta of beam kaon and scattered kaon, K1.8 beam line and KURAMA spectrometers were used, respectively. In addition, a position and an angle of the produced Ξ^- were measured with silicon strip detectors (SSD) which were located between the target and the nuclear emulsion. Hyperfragments emitted from the Ξ^- hyperon absorption points were observed with the nuclear emulsion detector. Charged particles emitted from the hyperfragments and escaping out of the emulsion stack were detected by two SSDs placed both upstream and downstream of the emulsion [18]. The Ξ^- hyperons are produced via the quasi-free p (K^-, K^+) Ξ^- reaction of K^- and diamond target.

2.4 Diamond target

The diamond was used to produce Ξ^- hyperons via the quasi-free p (K^-, K^+) Ξ^- reaction. The cross section of the (K^-, K^+) reaction is reported to be proportional to $A^{0.38}$ of the target material [19] but the produced Ξ^- is absorbed in nuclei particularly with a large Z. The target was also used as a degrader in order to stop the incoming Ξ^- in the emulsion located at the downstream of the target. Thus, a diamond target was employed since it has a high density. The diamond target has the size of 50.6-mm wide, 30.3-mm high and 30.4-mm thick. The volume and weight were 46.679 ± 0.225 cm^3 and 151.40 g, respectively. The density was calculated to be 3.243 ± 0.016 g/ cm^3. The produced Ξ^- particles are irradiate on the emulsion stack or module.

Chapter 3

Analysis

3.1 Ξ^- track following

Developed emulsion sheets were scanned by microscope scanning systems. The microscope systems consisted of an image sensor, a movable stage controlled by a computer, and optics. The emulsion sheet was fixed on the glass stage by vacuum pumping in the observation. The Z-axis of the coordinate system of the scanning was defined to the thickness direction. The stage is moved by stepping motors on XY axis recording its position with position encoders with a resolution of 1μm attached on the rails. The brightness of microscope images was controlled by an LED which was attached under the stage. Silicone immersion oil was poured on the emulsion sheet to use oil-immersion objective lenses. Z position of the focal plane was tuned by moving the objective lens by a stepping motor. Its position was also recorded with a position encoder with a resolution of 0.1μm. Optical images in the emulsion sheet were read by the CCD sensor through the objective lens. Several magnification types of objective lenses were used depending on the situation. Photographs obtained with the image sensor were recorded in pixel data which have 512(X) × 440(Y) pixels.

From the sets of the predicted position and angle of the Ξ^- hyperons given with the SSD, they were traced through the emulsion sheets with automated microscope scanning systems [20]. At first, the most upstream sheet of an emulsion module was scanned to find the Ξ^- tracks. Once found, the Ξ^- track was traced to downstream through several emulsion sheets. When the microscope system detected the end point of the track in the sheet, the system took pictures around the Ξ^- stopping point and those were examined by human eyes and categorized into the following groups. Schematic drawings of each group are shown in figure 3.1.

(1) ρ-stop: The Ξ^- track stop without nuclear fragments. The track became dizzy near the stopping point.

(2) σ-stop: The Ξ^- track stop with any nuclear fragment. The track became dizzy near the stopping point.

(3) Ξ^- decay: $\Xi^- \rightarrow \Lambda + \pi^-$ decay event. The straight Ξ^- track disappeared and π^- track is started from the end point.

(4) secondary interaction: The in-flight interaction between Ξ^- hyperon and a nucleus in the emulsion. The straight Ξ^- track is connected to nuclear fragments.

(5) beam interaction: The misidentification of Ξ^- track. The followed track is a fragment from an interaction between K^- beam and a nucleus in the emulsion. The followed track is connected to a star event caused by the K^- beam.

(6) through: The Ξ^- track penetrate all emulsion sheets.

(7) others

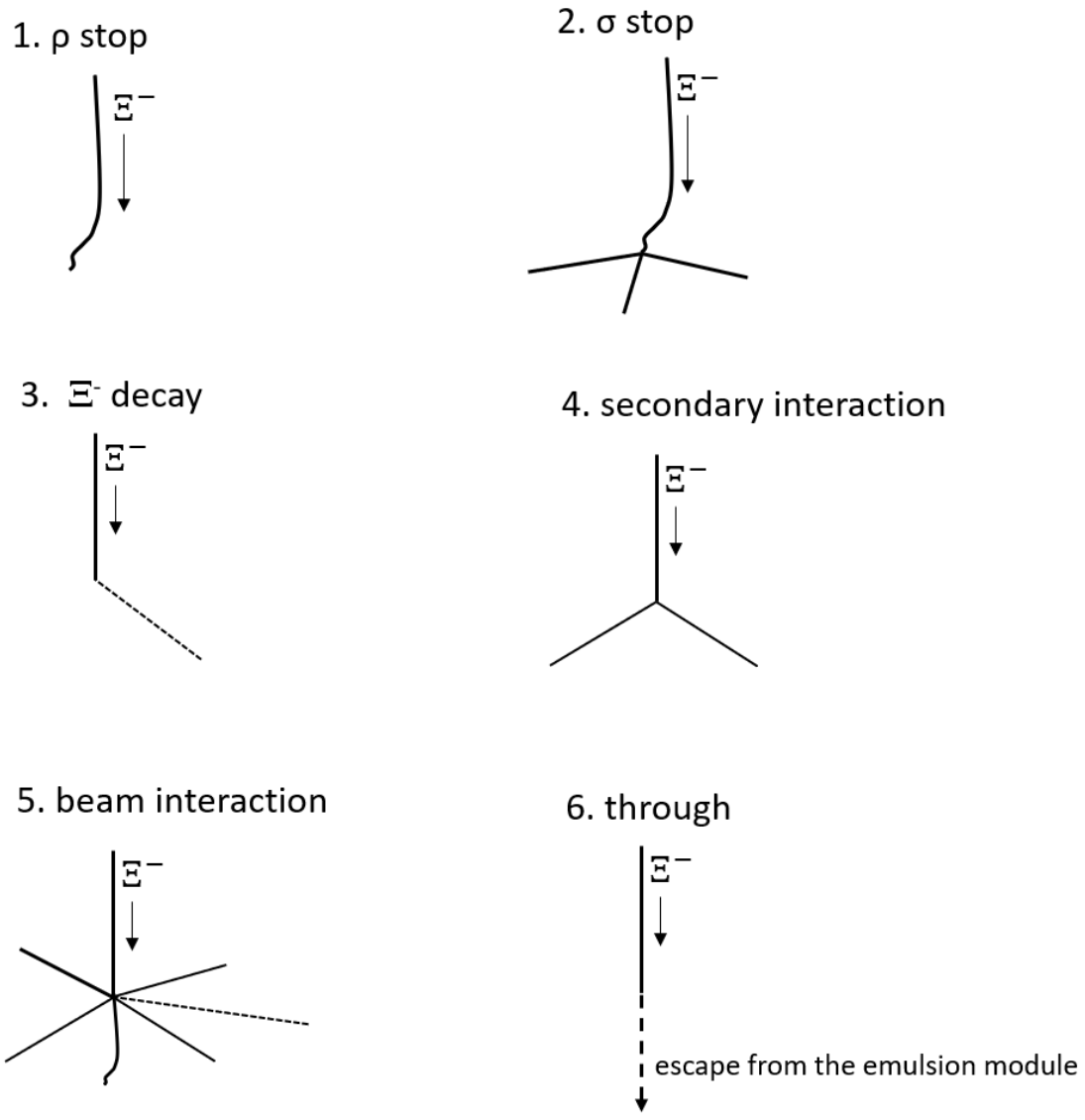

Fig 3.1. Schematic drawings of Ξ^- track categorization. An arrow in each drawing shows the direction of the track.

After an impressive event is observed, such an event was carefully analyzed to identify the nuclear species. The ranges and angles of the tracks were measured by fitting tracks around the vertices in the image analysis. The energies of the daughter particles were estimated from the ranges of the tracks with the Range energy formula. Possible nuclide combination was selected by checking the kinematic constraints at each vertex.

3.2 Range and angle measurement

Precise measurement for a special event is performed by a dedicated image processing for a series of micrographs. The micrographs are taken under 100x objective lens with a resolution of about 0.143 μm/pixel. Usually, several hundred micrographs were taken for an observed event by changing the focal plane to capture enough volume around the event. A typical interval of micrographs is 0.2μm in direction of the light-axis. Furthermore, we use several series of micrographs, typically 5 times, to estimate measurement reproducibility and error.

Our image processing is done by following procedures. At first, basic image processing is performed for the taken micrographs in order to distinguish track against the background: high-pass filtering, so-called "Difference of Gaussian", and brightness thresholding. Secondary, we roughly define the range and angle of the tracks visually by mouse-click action by a dedicated GUI-tool. Then, further processing is automatically performed as the following steps. The tracks are divided into short segments every 10 μm for a line fitting because tracks are not straight due to multiple Coulomb scattering. For each segment, about ten points on it are defined as "the core of the track" by the brightness gradient. Finally, a linear fitting is performed for the segments to minimize chi-square value. These "core finding" and "linear fitting" are iterated until the parameters converge.

The range measurement is essential to calculate the kinetic energy of particles. The track range before shrinkage is calculated by summing the segmented ranges as following.

$$R_i = \sum_{i=1}^{n} \sqrt{\Delta x_i^2 + \Delta y_i^2 + (SF \times \Delta z_i)^2} \tag{3.1}$$

$$R = \sum_{\mathrm{i}=1}^{4} R_i \tag{3.2}$$

where, Δx_i, Δy_i, and Δz_i represent the length of the i-th segment of a track, and SF is the shrinkage factor. For the case that a track passes through the polystyrene base, the equivalent range in base to that of emulsion is calculated by multiplying the correction factor (r).

$$R_b = r * \sqrt{(\Delta x_{\mathrm{b}})^2 + (\Delta y_{\mathrm{b}})^2 + (\Delta z_{\mathrm{b}})^2} \tag{3.3}$$

$$R = R_b + \sum_{i=1}^{5} R_i \quad (3.4)$$

The correction factor (r) of about 0.5 was used in our J-PARC E07 experiment. The factor is depending on the distance from the stop point and obtained by "SRIM 2013". Figure 3.2 demonstrates the measurement method of long and/or curved track in the emulsion layer and passes through the polystyrene base. The emission angle of a particle, θ as zenith and ϕ as azimuthal angle, are also obtained by the linear fitting in order to calculate the momentum vector. Typically, 10 μm length from the vertex point is used for the fitting for angle definition.

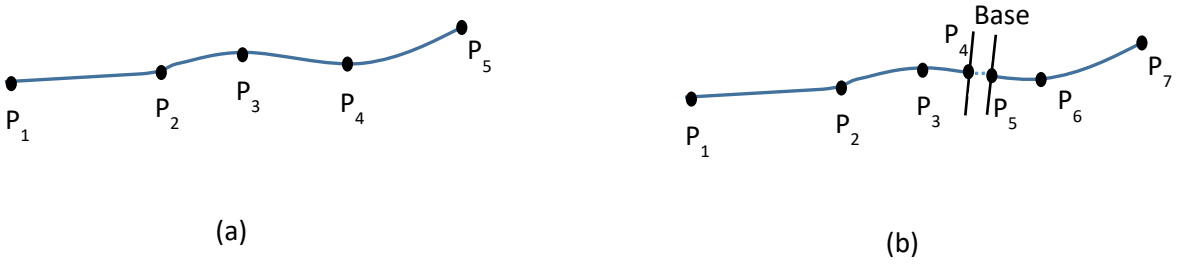

Fig 3.2. Schematic drawing of the segmented-measurement of a long and/or curved track. (a) A track in the emulsion layer. (b) A track passes through the polystyrene base.

3.3 Range-energy relation

The kinetic energy of a charged particle stopped in an emulsion layer is obtained by the following range-energy formula given by Barkas et. al., [21, 22].

$$R = \frac{M}{Z^2} \cdot \lambda(\beta) + R_{ext} \quad (3.5)$$

where, R, Z, and M are respectively the range of the track, charge, and mass of the particle in the unit of the proton mass. $\lambda(\beta)$ represents a range of a proton at the velocity of β in the standard emulsion, Ilford G5 emulsion with the density of 3.815g/cm^3. The R_{ext} means a range extension caused by electron capture for particles with multiple positive charges. This function is described as follows.

$$R_{ext} = MZ^{2/3} C_Z(\beta/Z) \quad (3.6)$$

where, C_Z, a function of β/Z, is an empirical one given by some experiments. The range of a particle depends on the density, in other words, the moisture content, of an emulsion layer. When the density of our emulsion is different from that of the standard emulsion, the following formula

is used to correct the range in a moisturized emulsion layer as a mixture of the standard emulsion and water by calculating the weighted harmonic average of their ranges.

$$\frac{\lambda_s}{\lambda} = \frac{rd-1}{rd_s-1} + \frac{r(d_s-d)}{rd_s-1} \cdot \frac{\lambda_s}{\lambda_w} \tag{3.7}$$

where, λ_s and λ_w are ranges of proton track in the standard emulsion and water, respectively. d and d_s are the density of our emulsion and that of the standard emulsion, respectively. r (=ΔV/ΔW) is the ratio of the volume increment, which has the unit of cm^3 /g, by the addition of moisture to an emulsion layer. It was measured as 0.884 for our emulsion layer.

The "range straggling effect" should be taken into account as an uncertainty of range-energy translation. Even if the energies of charged particles are monochromatic, their ranges vary stochastically. The main contribution to range straggling is that caused by electron collision. This effect is given by Barkas as a numerical table. These functions such as C_Z, λ_s, $\frac{\lambda_s}{\lambda_w}$, and "range straggling caused by electron collision" are expressed as polynomial functions in our software library.

3.4 Range energy calibration

The range depends not only on the particle energy but also on the emulsion density. The measured range must be corrected in depth direction because the thickness of an emulsion sheet is reduced to about a half of the original one after the photographic development. Figure 3.3. demonstrates the condition of emulsion sheet before and after photographic development. In order to measure the density and shrinkage factor of an emulsion sheet, decay alpha particles in the emulsion layer are used. Although these values are able to obtain by mechanical measurements, the way with alpha particles is the best solution to minimize the systematic uncertainties.

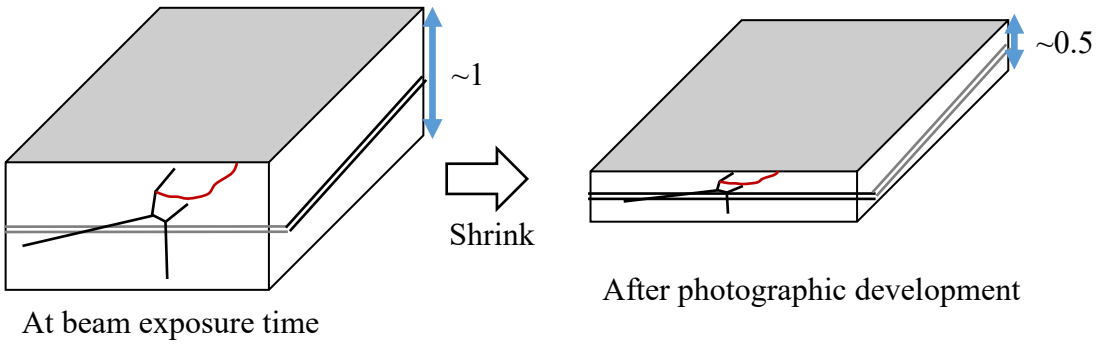

Fig 3.3. Schematic drawing emulsion sheet before and after photographic development.

We usually use the alpha tracks with the monochromatic energy of 8.784 MeV from decays of ^{212}Po. They are originated from natural isotopes of Thorium (^{232}Th) distributing in an emulsion layer randomly. They can be identified easily because they have a characteristic topology: the longest track in "alpha-star" having 5 alpha tracks. Figure 3.4 represents the flow chat of alpha decays of Thorium series. Figure 3.5 is the microscopic image of alpha tracks of thorium. A modern scanning technique, "Overall scanning method" is used for the alpha decay search [23].

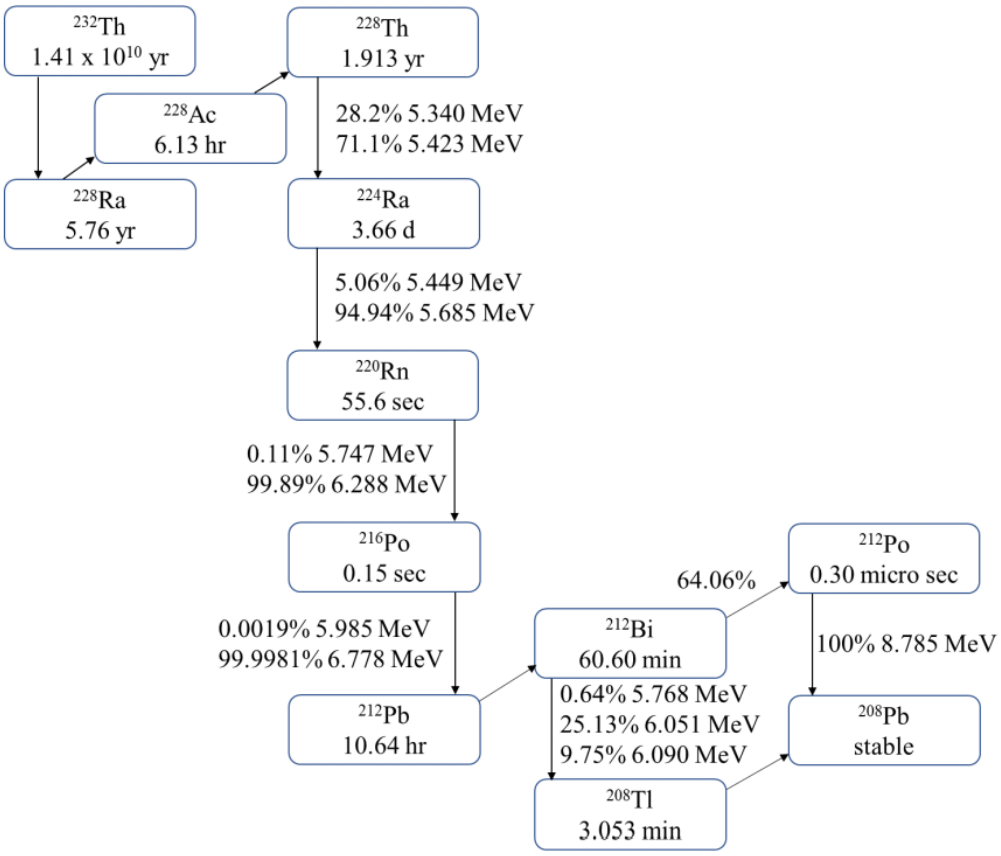

Fig.3.4. Thorium decay series.

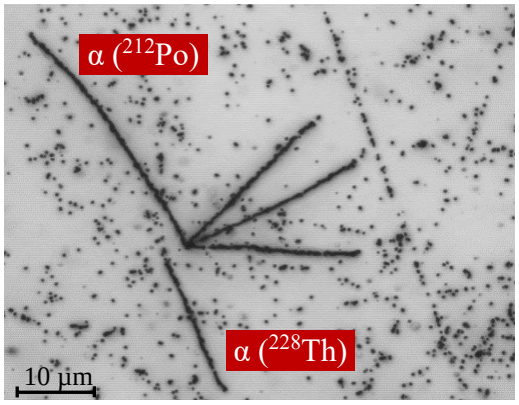

Fig 3.5. Microscopic images of alpha particles from Thorium series.

3.4.1 Overall Scanning Method with Vertex picker

Regarding a hybrid method with nuclear emulsion, the production of double-Λ hypernuclei is strongly depend on the detection efficiency of K^+ mesons tagged by KURAMA spectrometer. The detection efficiency of Ξ^--hyperons in the first plate of emulsion module is about 50% due to the tagging efficiency of a K^+ spectrometer, and the non-uniformed space between the surface of first emulsion plate and SSD detectors. However, un-trigged typical events would be recorded in nuclear emulsion since Ξ^--hyperons are also produced via some other process such as n'(K^-, K^0) Ξ^-, where K^0 are not tagged by KURAMA.

In the same way, the data on production, position, and production-time of alpha in emulsion layers could not be recoded. Because, the alpha decay event originated from natural isotopes of the Thorium series in the emulsion included as impurities of emulsion materials. Therefore, the work of conventional scanning of alpha-particles in emulsion layer with human's eyes, so-called eye-scan, under a microscope was performed. It is necessary to collect at least about one hundred events of alpha decays in order to calibrate range-energy relation for a special event. The conventional scanning method took half to one hour to find an alpha decay event with eye-scan. This conventional search is heavy labor for the scanner and time-consuming method.

A new searching or scanning method was developed to speed up the detection of alpha decay vertices as shown in figure 3.6. In this method, (i) a computer-controlled optical microscope scans emulsion layers exhaustively and a high speed, high resolution camera takes the microscopic images of the tracks, and (ii) a dedicated image processing procedure is applied to pick out vertex-like events which has characteristic topology with multi tracks and vertices. We named the method

as “Overall scanning” because this method scans the entire volume of emulsion sheets. This method was widely expressed in [23].

Several ten thousand of images of vertex-like events were taken by the Vertex Picker in one emulsion layer (~ 500 µm before development process) of the area of 5 × 5 cm^2. These output images are mixing images of alpha, beam interaction, one-vertex, two-vertexes, three-vertex (very small percentage compared to other events), cross track, black dot trash, etc. These images were classified by human eye with the help computer software called Classification Viewer. The images of two vertex and three vertex candidates, and alpha decay candidates for Thorium are selected. The classified images of alpha decay were confirmed by setting the corresponding emulsion plate on the microscopic stage and checking by human-eye. Only the fine, bold and long-track alpha decays events were selected. Then, we set the data (x-, y-, z-coordinates values) of these alpha decays to the computer programing code and took their images automatically with 100 times objective lens. The track-ranges of the longest alpha tracks (alpha decays of ^{212}Po) were measured and used for range-energy calibration.

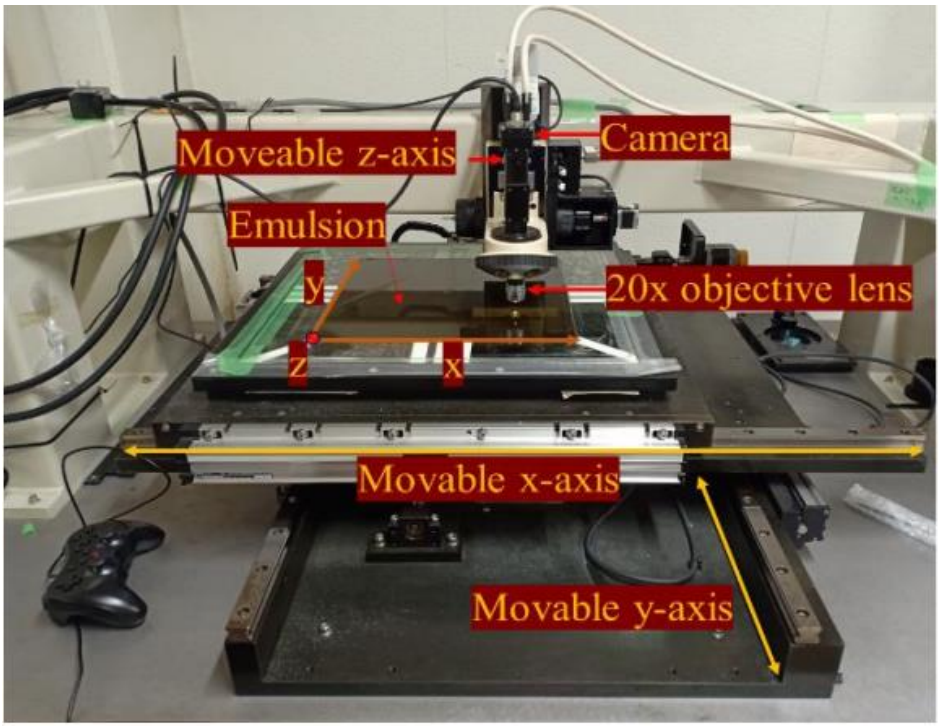

Fig 3.6. Microscopic system for Vertex Picker

3.4.2 Shrinkage factor and emulsion density measurement

For instance, for the 4th sheet in module #098 in which "D001 event" [25] exist, we collected about 140 alpha-tracks and measured their ranges using the "Overall viewer1" with the image processing procedure. Using these measured data of the range of alpha-tracks were calculated using the equation (3.1). In this calculation, the shrinkage factor (*SF*) was applied as a variable in the calculation of track-range of α-particle, and it was assigned to give the smallest standard deviation (*Stdev.*) of the range as shown in figure 3.7 (a). The mean range (*R*)in the emulsion sheet before development was recalculated with the assigned value of *SF* as presented in figure 3.7 (b). The *SF* and *R* values were obtained to be 1.881 ± 0.012 and 49.46 ± 0.12 μm, respectively. The *R* value of 49.46 ± 0.12 μm is the equivalent range to 8.784 MeV of its energy. From this the coefficient of range-energy relation, density of emulsion sheet, was determined to be 3.635 ± 0.014 g/cm^3.

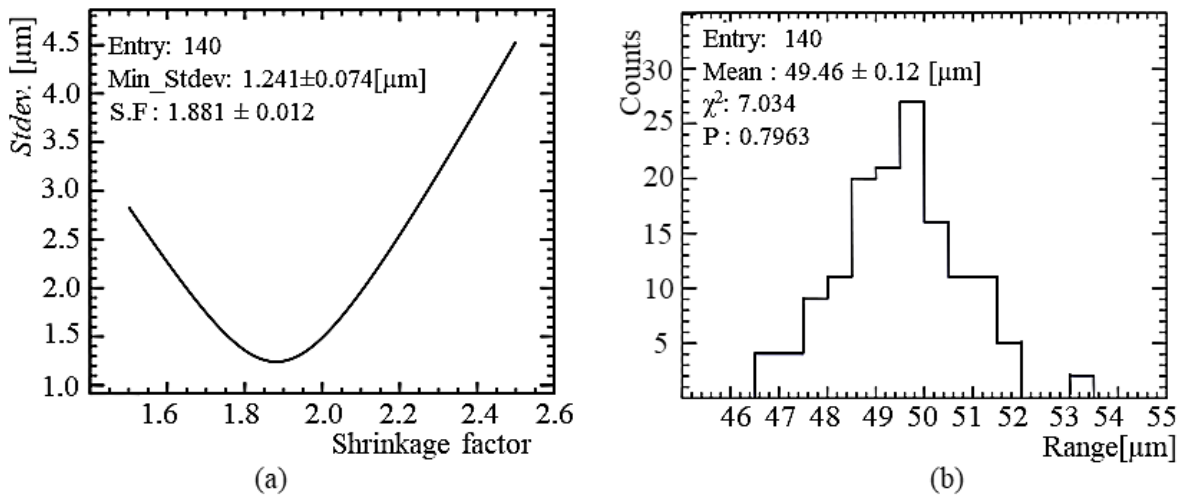

Fig 3.7. (a) Error of the α-range distribution as a function of *SF*. (b) Distribution of α range for the assigned *SF* of 1.881.

The *SF* and emulsion density are the significant parameters in events analysis and they are slide different in plate to plate even in the same emulsion module. The *SF* and emulsion density of each emulsion plate in which the analyzed events are detected, are necessary to measure. Therefore, the *SF* and emulsion density of emulsion plates of 10th plate of module 047 and 5th plate of module 019 in which "IBUKI event" [26] and "IRRAWADDY event" [26, 28] were detected and measured by the same method as described above. Table 3.1 summarized the *SF* and emulsion density of the emulsion plates in which the typical events are detected.

Table 3.1 The calibration coefficients of the corresponding typical events.

Quantity	**Events**		
	D001	IBUKI	IRRAWADDY
Emulsion plate	Mod: 098, Pl: 04	Mod: 047, Pl: 10	Mod: 019, Pl: 05
Number of alpha decays	140	125	165
SF	1.881 ± 0.012	2.078 ± 0.021	1.872 ± 0.014
R [μm]	49.46 ± 0.12	50.25 ± 0.11	48:79 ± 0.10
Emulsion density [g/cm^3]	3.635 ± 0.014	3.544 ± 0.012	3:714 ± 0:012

3.5 Event reconstruction

We perform event reconstruction to identify the nuclide of a double strangeness system. At first, we assign all the possible particle to each track. Then, for each track, the kinematic energy is defined by range-energy relation. The momentum vector is also doing by energy-momentum translation. Secondly, we check the kinematic consistency for the all-possible combinations. If a single reasonable interpretation is survived, the nuclide is identified successfully.

The considered case is summarized in Table 3.2. As the initial state, Ξ^- capture at rest, three cases are listed: Ξ^- +^{12}C, ^{14}N, or ^{16}O, which are the medium-heavy nucleus in an emulsion layer. For each reaction, neutral particles emission is also considered. 41 kinds of single-Λ hypernuclei and 40 double-Λ hypernuclei are listed. The mass of some SH is an estimated by linear-extrapolation using by that of several isotopes of single-Λ hypernuclei. The mass of double-Λ hypernuclei is estimated by single-Λ hypernuclei with the condition of $\Delta B_{\Lambda\Lambda} = 0$.

Table 3.2: Particles table considered in the event reconstruction

Type	No. of case	Particle or nuclide
Initial state	7	$\Xi^- + {}^{12}$C, ^{13}C, ^{14}N, …, ^{17}O, or ^{18}O
Daughters without strangeness	65	π^-, p, d, t, ^{3}He, ^{4}He, …,^{19}N, or ^{19}O
Neutral particles	10	n, 2n, 3n,π^0,π^0+n,π^0+2n, Λ, Λ+n, Λ+2n or more
Single-Λ hypernucleus	41	${}^{3}_{\Lambda}$H, ${}^{4}_{\Lambda}$H, ${}^{4}_{\Lambda}$He, …, ${}^{17}_{\Lambda}$N, or ${}^{18}_{\Lambda}$N
Double-Λ hypernucleus	40	${}^{4}_{\Lambda\Lambda}$H, ${}^{5}_{\Lambda\Lambda}$H, ${}^{5}_{\Lambda\Lambda}$He, …, ${}^{17}_{\Lambda\Lambda}$N, or ${}^{18}_{\Lambda\Lambda}$N

These calculations are implemented in Python-language. The processing time to evaluate a 3-prong decay is less than 5 minutes on a typical PC.

Particle ID with track feature is important to refine the event reconstruction. The grain density and boldness of tracks have information on *dE/dx* of the particle in the emulsion layer. For a track having about 100 μm range, charge ID method developed by Kinbara [24] is applied. Furthermore, the feature of the track endpoint has plenty of information. If an electron-like track is seen from there, it shows the nucleus occurred a β-decay. In the case of a "hammer track", it is one of the A=8 nuclei. A π^- track has characteristic features: thin and straight around the emitting point, however dense and dizzy near the stop point, and a few nuclear fragments are often seen at the stop point.

For an identified event, mass calculation of double strangeness system is performed. The mass of a DH is reconstructed by energy conservation in the production and decay process, i.e., $M(Z') + M(\Xi^-) - B_{\Xi^-} = M({}_{\Lambda\Lambda}Z) + K.E.({}_{\Lambda\Lambda}Z) + \sum M_{\text{other}} + \sum K.E_{\text{other}}$, and $M({}_{\Lambda\Lambda}Z) = \sum M_{\text{daughter}} + \sum K.E._{\text{daughter}}$, respectively. Usually, the value of B_{Ξ^-} is used that of 3D state of Ξ^- in Z' = C, N, or O. Finally, $B_{\Lambda\Lambda}$ of a double hypernuclei is defined as the difference between $M({}^{A}{}_{\Lambda\Lambda}Z)$ and $M({}^{A-2}Z) + 2M(\Lambda)$.Also, B_{Ξ^-} of Ξ event are reconstructed by $M(Z') + M(\Xi^-) - B_{\Xi^-} = E_{\text{final state}}$, where, two single Λ hypernuclei must be seen in the final state, i.e., the event must be twin hypernuclear event.

Chapter 4

Interpretation of the D001 event, IBUKI event, and Irrawaddy event

In E07 experiment, 33 double hypernuclear events have been detected with counter-hybrid emulsion method for two years from April 2018 to March 2020. Among these events, two double-Λ hypernuclear events, MINO [9] and D001 [24], and a twin single- Λ hypernuclear event, IBUKI [25], have been analyzed and reported. Another twin single- Λ hypernuclear event, IRRAWADDY [26, 27], was already analyzed and the result will be reported in very near future. In this chapter, the detail analysis of the three events (D001, IBUKI, and IRRAWADDY) as described above were presented. The other double-hypernuclear events are now under the analysis processes.

4.1 Analysis of the D001 event

4.1.1 Event description

The event with three vertexes topology was detected in the downstream of 4th plate of Module no. 98 of the emulsion stacks. According to the characteristics of sequential decay topology of this event, it was denoted as double-Λ hypernuclear event and named as D001 [25].

A superimposed image and schematic drawing of the D001 event are shown in figure 4.1. The image is the superimposed image of a few hundred of micrograph taken at various focusing depths of the microscope in the emulsion layer. A Ξ^- hyperon came to rest at point A, from which two charged particles (track#1, and #3) were emitted. The track #1 denoted as double-Λ hypernucleus which decayed into a single-Λ hypernucleus (track #2) and another charged particle (track #4) at point B. This single-Λ hypernucleus of track #2 decayed sequentially to two ordinary-charged particles (tracks #5, and #6) at point C.

The measured track lengths and emission angles of the D001 event are summarized in Table 4.1. The track lengths measurement was carried out as presented in Section 3.2. The measurement of very short tracks, tracks #2 and #5, give the large error measurement value. One of the long tracks, track #4, was stopped in the upstream of 2nd plate of that module with ρ-stop. Another long track, track #6, was dissipated it energy in going to the downstream direction, and stopped with ρ-stop also in the down layer of the next plate, 5th plate, of that module. Since the particles #4 and #6 were going through the PS film base, the segmented length in the base were

converted to the equivalent lengths in the emulsion layer. In each vertex point of production and decays, two daughter particles were associated, respectively.

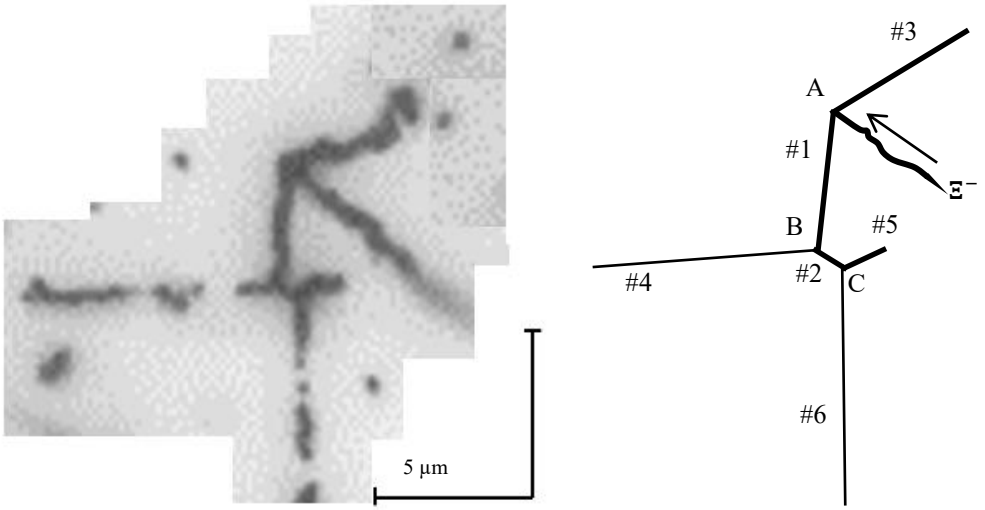

Fig 4.1. Superimposed image (left) and schematic drawing (right) of the D001 event.

Table 4.1: The measured track ranges and emission angles of the D001 event. Angles are expressed by a zenith angle (θ) with respect to the direction perpendicular to the plate and an azimuthal angle (ϕ). The indicated errors are the measurement errors only. For tracks #4 and #6, the track ranges in PS film base were converted to those in the emulsion layer.

Vertex	Track	R [μm]	θ [deg]	ϕ [deg]	Comments
A	#1	4.1 ± 0.3	53.6 ± 3.6	82.7 ± 2.8	double-Λ hypernucleus
	#3	5.5 ± 0.4	140.3 ± 2.1	188.4 ± 2.7	
B	#2	1.1 ± 0.2	33.7 ± 15.5	153.3 ± 20.2	single-Λ hypernucleus
	#4	5728.6 ± 5.9	108.9 ± 2.4	2.2 ± 2.0	
C	#5	1.8 ± 0.5	50.6 ± 6.7	187.4 ± 9.1	
	#6	1762.6 ± 2.6	55.1 ± 1.9	91.5 ± 1.6	

4.1.2 Calculation of the ΛΛ binding energy

From the kinematic calculation at the production or decay point of a double-Λ hypernucleus, the mass of the double-Λ hypernucleus, $M\left({}^{A}_{\Lambda\Lambda}Z\right)$, can be determined. Then, the values of $B_{\Lambda\Lambda}$ and $\Delta B_{\Lambda\Lambda}$ are measured as follows:

$$B_{\Lambda\Lambda}\left({}^{A}_{\Lambda\Lambda}Z\right) = M\left({}^{A-2}Z\right) + 2M(\Lambda) - M\left({}^{A}_{\Lambda\Lambda}Z\right), \quad (4.1)$$

$$\Delta B_{\Lambda\Lambda}\left({}^{A}_{\Lambda\Lambda}Z\right) = B_{\Lambda\Lambda}\left({}^{A}_{\Lambda\Lambda}Z\right) - 2B_{\Lambda}\left({}^{A-1}_{\Lambda}Z\right), \quad (4.2)$$

where, Z, A and *M* are the charge, baryon number, and mass, respectively. The B_{Λ} is the Λ binding energy of a single hypernucleus of ${}^{A-1}_{\Lambda}Z$. It should be noted that, at the production point, the $B_{\Lambda\Lambda}$ and $\Delta B_{\Lambda\Lambda}$ values depend on the Ξ^- binding energy, B_{Ξ^-}, which is defined as:

$$B_{\Xi^-} = M\left({}^{A}Z\right) + M(\Xi^-) - M[{}^{A+1}_{\Xi}(Z-1)], \quad (4.3)$$

where, $M[{}^{A+1}_{\Xi}(Z-1)]$ represents the mass of an atomic bound system of Ξ^- and the core nucleus. Therefore, the values of $B_{\Lambda\Lambda} - B_{\Xi^-}$ were obtained.

4.1.3 Event reconstruction

The production and decay processes of the D001 event were reconstructed by energy and momentum conservation obtained from the ranges and emission angles of daughter particles. If the momentum sum of the daughter particles was deviated from zero by more than 3 standard deviations (3σ), the mode will be rejected. At the production point A, the kinematics consistency of all possible modes was checked by assuming that Ξ^- hyperon was captured at atomic 3*D* state of the medium-heavy nuclei such as ^{12}C, ^{14}N, or ^{16}O. If the Ξ^- hyperon was captured in a heavy nucleus such as Ag or Br, a short track like track #3 with a range of less than 32 μm could not be emitted due to the Coulomb barrier [5]. According to the topology of not back-to-back of the emitted direction of the two tracks, the corresponding momenta were not conserved at all vertices A, B and C. Therefore, at least one neutral particle will be emitted in the reaction process of this event. Furthermore, the stopping points of tracks #4 and #6, although they were long-range tracks, did not show the topology of π^- stopping such as emission of auger electrons and/or nuclear fragments as interpreted in the section 4.2.1. By this condition, the possibility of tracks #4 and #6 as π^- particles were rejected.

The possible production modes at point A were nominated with the criterion of $\Delta B_{\Lambda\Lambda} - B_{\Xi^-}$ between -5 MeV and +5 MeV within 3σ. The B_{Ξ^-} of the of Ξ^- hyperon captured at atomic

3*D* state of the ^{12}C, ^{14}N, or ^{16}O was represented to be 0.1 to 0.2 MeV [30], and it was negligible small. So that the criterion was emphasized on $\Delta B_{\Lambda\Lambda}$. From the previous experiment, E373, the $\Delta B_{\Lambda\Lambda}$ was measured to be nearly +2 MeV as maximal. Therefore, the upper limit of the criterion was set by 5 MeV. In order to cover all possible modes, including the repulsive case of $\Lambda - \Lambda$ interaction, the lower limit was set to -5 MeV. The possible production modes after discriminated by this criterion were listed in Table 4.2.

Table 4.2: Possible production modes at point A of the D001 event. The error value was obtained from the measurement error.

No.	Ξ^- captured		#1	#3		$B_{\Lambda\Lambda} - B_{\Xi^-}$ [MeV]	$\Delta B_{\Lambda\Lambda} - B_{\Xi^-}$ [MeV]
1.	$\Xi^- + {}^{12}\mathrm{C}$	$\rightarrow$	${}^{\ 8}_{\Lambda\Lambda}\mathrm{Li}$	${}^4\mathrm{He}$	n	17.50 ± 1.46	6.34 ± 1.46
2.	$\Xi^- + {}^{14}\mathrm{N}$	$\rightarrow$	${}^{10}_{\Lambda\Lambda}\mathrm{Be}$	${}^4\mathrm{He}$	n	15.05 ± 2.78	1.63 ± 2.78

At point B, the double-Λ hypernucleus (track #1) decayed into a single-Λ hypernucleus (track #2) and a nuclear fragment (track #4). The cases of double-hypernuclei with 3 to 6 units of charge and baryon mass number less than 15 units were emphasized because we considered that Ξ^- particle was captured by ^{12}C, ^{14}N, or ^{16}O nucleus, and track #4, track #5 and/or track #6 has no pion-like track topology as described above. The decay modes with neutron emission were dominant as we presented above. For the decay modes with one neutron emission, the limits of the nominated criterion of $\Delta B_{\Lambda\Lambda}$ was set between −5 MeV and +5 MeV within 3σ. For the modes with multiple-neutron emission, we could measure only the minimum momentum of the neutrons because each directions of emitted neutrons could not be specified. From this, the minimum value of $\Delta B_{\Lambda\Lambda}$ will be measured. Thus, the upper limit of criterion, +5 MeV, was not set. In total, there were 42 possible decay modes of ${}_{\Lambda\Lambda}$Li, ${}_{\Lambda\Lambda}$Be, ${}_{\Lambda\Lambda}$B, and ${}_{\Lambda\Lambda}$C at point B. Among these possible decay modes, the ones ${}^{\ 8}_{\Lambda\Lambda}$Li and ${}^{10}_{\Lambda\Lambda}$Be which were consistent with the result of point A were listed in Table 4.3.

A comparison of the values of $B_{\Lambda\Lambda}$ to the number of baryons, A(${}_{\Lambda\Lambda}$Z), for the candidates of the D001 event listed in Table 4.3 to the ones taken from the previous events [5, 8, 9] was represented by figure 4.2. Since the plotting point of case No.1 (${}^{\ 8}_{\Lambda\Lambda}$Li) in Table 4.3 was far from the line of $B_{\Lambda\Lambda}$ to A(${}_{\Lambda\Lambda}$Z), the case No.2 (${}^{10}_{\Lambda\Lambda}$Be) seems most likely to be the nuclide of the D001 event.

Table 4.3: Possible decay modes at vertex B of D001 event.

No.	DLH (#1)		#2	#4		$B_{\Lambda\Lambda}$ [MeV]	$\Delta B_{\Lambda\Lambda}$ [MeV]
1.	${}^{8}_{\Lambda\Lambda}$Li	→	${}^{4}_{\Lambda}$He	p	3n	<106.68 ± 0.90	<95.52 ± 0.90
2.	${}^{8}_{\Lambda\Lambda}$Li	→	${}^{4}_{\Lambda}$He	d	2n	<62.21 ± 2.53	<51.05 ± 2.53
3.	${}^{8}_{\Lambda\Lambda}$Li	→	${}^{5}_{\Lambda}$He	p	2n	<123.14 ± 1.36	<111.98 ± 1.36
4.	${}^{10}_{\Lambda\Lambda}$Be	→	${}^{6}_{\Lambda}$Li	p	3n	<104.29 ± 1.27	<90.64 ± 1.27
5.	${}^{10}_{\Lambda\Lambda}$Be	→	${}^{6}_{\Lambda}$Li	d	2n	<62.17 ± 3.42	<48.52 ± 3.42
6.	${}^{10}_{\Lambda\Lambda}$Be	→	${}^{7}_{\Lambda}$Li	p	2n	<106.91 ± 1.93	<93.26 ± 1.93
7.	${}^{10}_{\Lambda\Lambda}$Be	→	${}^{7}_{\Lambda}$Li	d	n	31.98 ± 6.65	18.33 ± 6.65

Therefore, the possible reaction of the D001 events was interpreted as:

$$\Xi^{-} + {}^{14}\mathrm{N} \rightarrow {}^{10}_{\Lambda\Lambda}\mathrm{Be} + {}^{4}\mathrm{He} + \mathrm{n}, \tag{4.4}$$

$$\hookrightarrow ({}^{6}_{\Lambda}\mathrm{Li} \text{ or } {}^{7}_{\Lambda}\mathrm{Li}), \text{ cases No.4 – 7 in Table 4.3.} \tag{4.5}$$

The single-Λ hypernucleus, ${}^{6}_{\Lambda}$Li or ${}^{7}_{\Lambda}$Li, in equation (4.5) has several possible decay modes with multiple-neutron emissions as listed in Table 4.4.

At vertex C, the decay of single-Λ hypernucleus (track#2) was identified by the reconstruction of its daughter particles (tracks #5 and #6). From all nuclide combinations for non-mesonic decays of known single-Λ hypernuclei, possible decay modes were discriminated. Track #5 with the short range could be accepted as particle with one or more unit of charge. Track #6 has more probability to a unit charged particle. If it has more than a unit of charge, the total kinetic energy of the two charged particles (#5 and #6) was much larger than the Q-value of any decay mode due to its long range. Therefore, the modes with the total kinetic energy larger than the Q-value will be rejected. Taking this into account and the most like case of sequential decay of ${}^{10}_{\Lambda\Lambda}$Be in Table 4.3, the possible decay mode of track #2 restricted to ${}^{6}_{\Lambda}$Li or ${}^{7}_{\Lambda}$Li were listed in Table 4.4.

Table 4.4: Possible decay modes of the single-hypernucleus (SLH).

SLH (#2)		#5	#6	neutral	Q [MeV]	B_Λ [MeV]
${}^{6}_{\Lambda}$Li	→	^{3}He	p	2n	153.006	<121.760
${}^{6}_{\Lambda}$Li	→	^{4}He	p	π^0 + n	38.606	<-1.739
${}^{7}_{\Lambda}$Li	→	p	^{3}He	3n	146.263	<10.925
${}^{7}_{\Lambda}$Li	→	^{3}He	p	3n	146.263	<118.936
${}^{7}_{\Lambda}$Li	→	^{3}He	d	2n	148.487	<94.008
${}^{7}_{\Lambda}$Li	→	^{4}He	p	2n	166.840	<135.387
${}^{7}_{\Lambda}$Li	→	^{4}He	p	π^0 + 2n	31.863	<1.213

In order to obtained the $B_{\Lambda\Lambda}$ and $\Delta B_{\Lambda\Lambda}$ for the production of ${}^{10}_{\Lambda\Lambda}$Be at vertex A, the B_{Ξ^-} value of 0.17 MeV for the atomic 3*D* state captured of Ξ^- hyperon in the the $^{14}\mathrm{N} + \Xi^-$ system [29] and the B_Λ of ${}^{9}_{\Lambda}$Be of 6.71 ± 0.04 MeV [30] was used. The mass of the Ξ^- and Λ hyperons were taken as 1321.71 ± 0.07 MeV and 1115.683 ± 0.006 MeV, respectively [31, 32]. The $B_{\Lambda\Lambda}$ and $\Delta B_{\Lambda\Lambda}$ were measured to be 15.22 ± 2.78 MeV and 1.80 ± 2.78 MeV, respectively. Although the error is as large as one order of magnitude for the data from the NAGARA and MINO event due to the neutron emission, the Λ-Λ interaction strength, $\Delta B_{\Lambda\Lambda}$, agrees with these two events.

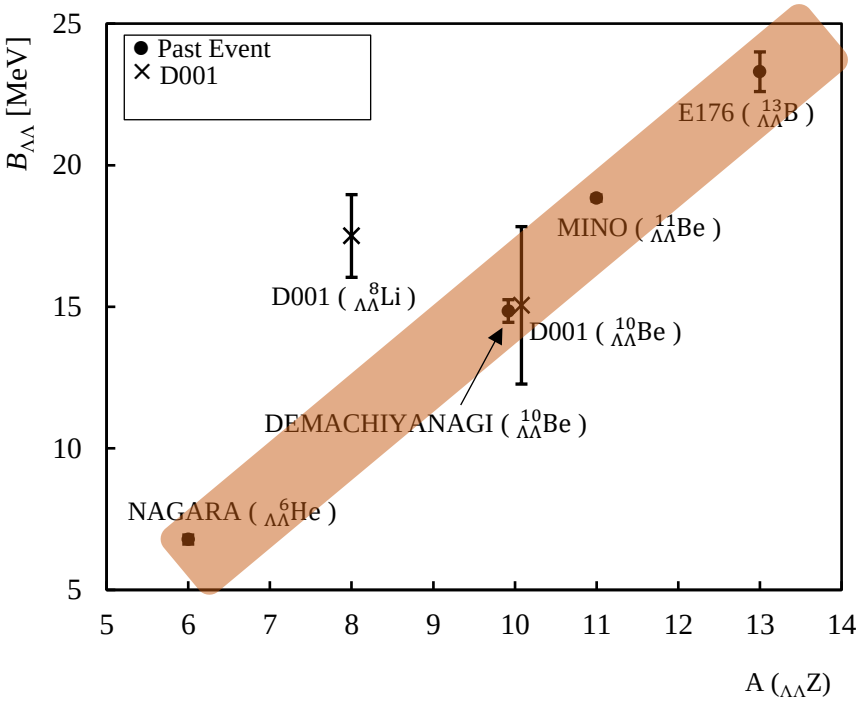

Fig 4.2. The $B_{\Lambda\Lambda}$ graph of observed DLH. The dots (●) and crosses (×) are obtained by the previous events and this event, respectively. With the exception of NAGARA, the past events show the most likely cases.

4.2 Analysis of the IBUKI event

4.2.1 Event description

The event with three vertexes topology was detected in the downstream of 10th plate of module no. 47 of the emulsion stacks. According to the characteristics of decay topology of this event, it was denoted as twin single-Λ hypernuclear event and named as IBUKI [26].

A superimposed image and schematic drawing of the IBUKI event are shown in figure 4.3. A Ξ^- hyperon came to rest at vertex A, from which two charged particles (tracks #1, and #2) are emitted back-to-back with each other (i.e., collinear). The track #1 decayed into four charged particles, tracks #3-6 at vertex B and track #2 decayed into three charged particles, tracks #7-9 at vertex C. Sine tracks #1 and #2 charged particles have a decay mode each, they are denoted as single-Λ hypernuclei. The hypernuclear event with the production of two single-Λ hypernuclei simultaneously is called twin single-Λ hypernuclear event.

All of the tracks are traced till their stopping points in the emulsion layer. Track #3 have a short range. All of tracks #3, #4, and #7 stopped in current plate. Track #5 going to the downstream

direction and stopped in 11th plate with ρ-stop. A thin track # 6 going to the upstream direction with long range and stopped in 3rd plate with ρ-stop. Track #8 is a thin track going to the downstream direction. In plate no.12th it becomes a bold track, and stop with the topology as shown in figure 4.4 which was interpreted as the σ-stop. A charged particle was emitted to the upper-left direction. Auger electron was also observed. Therefore, track #8 was identified as a negative-charged particle, π^- meson. The stopping point of track #9 was observed in the 9th plate as the ρ-stop. Then, the analysis processes of the IBUKI event were carried out.

The range measurement of short tracks within a microscopic view was performed with the manner described in Section 3.2. In order to avoid an effect of distortion aberration, images of track #2 were divided into two data sets. In the case of long tracks out of a microscopic view, the tracks were manually traced to the stopping points. The positions of the points on the track were measured at intervals of around 50 μm. The range of long tracks was calculated as the length of a polygonal line. Table 4.5 summarizes the measured ranges and the emission angles of all tracks. The angles are expressed by a zenith angle (θ) and an azimuthal angle (ϕ) in respect to the angle perpendicular to the emulsion sheet. For track #6, #8, and #9, the ranges in a base film were converted to those in the emulsion layer.

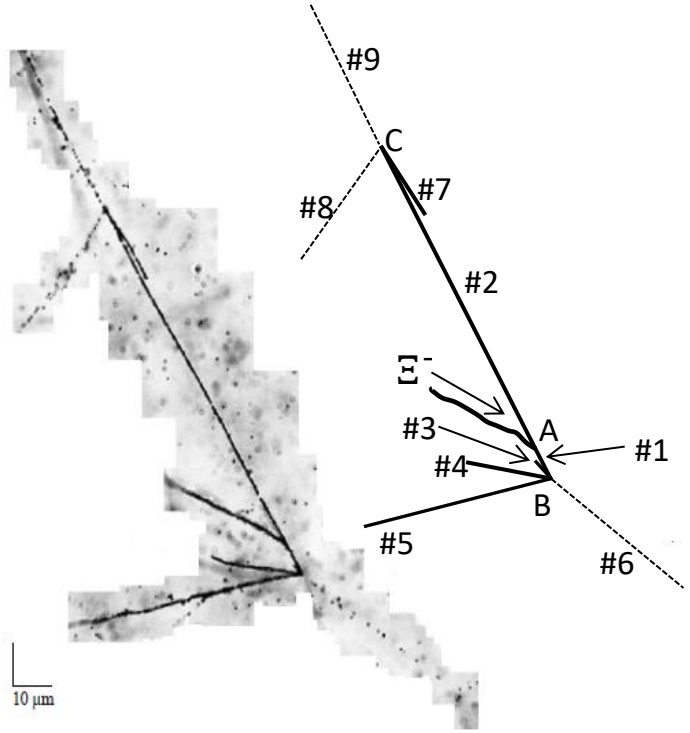

Fig 4.3. Superimposed image (left) and schematic drawing (right) of the IBUKI event.

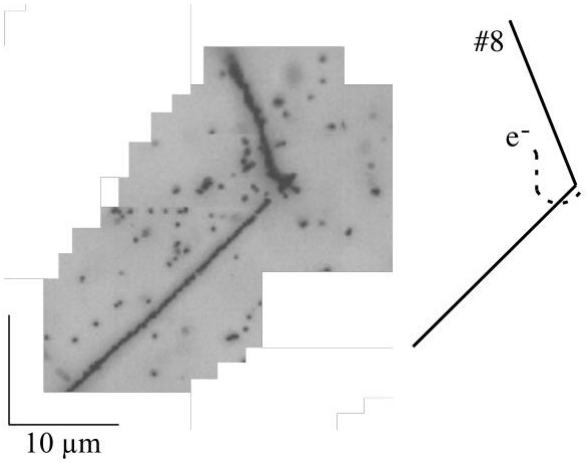

Fig 4.4. Superimposed image of the end point of track #8. A charged particle was emitted with the range of 178.13 ± 1.04 μm form the end point of #8 and auger electron was observed.

Table 4.5: The measured track ranges and emission angles of the IBUKI event.

Vertex	Track	R [μm]	θ [deg]	ϕ [deg]	Comments
A	#1	8.2 ± 0.4	90.6 ± 1.9	301.9 ± 2.1	Single hypernucleus
	#2	88.5 ± 0.3	93.5 ± 2.0	122.9 ± 1.5	Single hypernucleus
B	#3	3.6 ± 1.1	124.6 ± 7.4	137.0 ± 6.4	
	#4	25.9 ± 0.3	109.8 ± 2.3	172.8 ± 1.5	
	#5	961.1 ± 4.6	49.6 ± 2.0	189.2 ± 2.0	
	#6	>20508 ± 33	111.6 ± 2.7	325.5 ± 2.2	
C	#7	19.2 ± 0.2	86.8 ± 1.6	307.0 ± 1.2	
	#8	2159.0 ± 19.1	30.6 ± 1.5	237.8 ± 2.8	π^- with σ-stop
	#9	2179.0 ± 3.6	106.7 ± 1.6	123.5 ± 1.2	

4.2.2 The kinematic fitting

The kinematic fitting is applied to each candidate [33]. This is based on the Lagrange multipliers method. Constraints are expressed as follows:

$$H(\alpha,\beta) = 0\ , \tag{4.6}$$

$$H_1 = \sum_{i=1}^{n}\sqrt{m_i^2 + p_i^2} - m_0\ ,$$

$$H_2 = \sum_{i=1}^{n} p_i sin\theta_i cos\phi_i\ ,$$

$$H_3 = \sum_{i=1}^{n} p_i sin\theta_i sin\phi_i\ ,$$

where, m, p, θ, and ϕ represent mass, momentum, zenith angle, and azimuthal angle, respectively. The subscript 0 corresponds to the parent nuclide and the others show i-th daughter nuclide. The known parameters (e.g., p_i, θ_i, ϕ_i) and unknown variables (e.g., a mass of double hypernuclei, a momentum of the particle which escaped from the emulsion) are denoted as α and β, respectively. Both of them are expressed as the vector with the length of a and b. The parameter b should be less than or equal to the number of constrains which is four in this case. Equation 3.1 constraints the conservations of the energy and the momentum at the decay event. Then, the linearized equations can be obtained as follows by expanding around a convenient point (α_A, β_A):

$$0 = \frac{\partial H}{\partial \alpha}|_{\alpha_A,\beta_A}(\alpha - \alpha_A) + \frac{\partial H}{\partial \beta}|_{\alpha_A,\beta_A}(\beta - \beta_A) + H(\alpha_A,\beta_A) \equiv D\eta + Ez + d, \tag{4.7}$$

$$D_{i,j} = \frac{\partial H_i}{\partial \alpha_j}|_{\alpha_A,\beta_A},$$

$$E_{i,j} = \frac{\partial H_i}{\partial \beta_j}|_{\alpha_A,\beta_A},$$

$$d_i = H_i(\alpha_A,\beta_A),$$

where, the dimensions of D and E are the $4 \times a$ and $4 \times b$, respectively. Then, the χ^2 can be defined as follows:

$$\chi^2 = (\eta - \eta_0)^t V_{\eta_0}^{-1}(\eta - \eta_0) + 2\lambda^t(D\eta + Ez + d), \tag{4.8}$$

$$\eta_0 = \alpha_0 - \alpha_A,$$

$$V_{\eta_0} = \begin{pmatrix} \sigma_1^2 & 0 & \cdots & 0 \\ 0 & \sigma_2^2 & \cdots & \vdots \\ \vdots & \vdots & \ddots & \vdots \\ 0 & 0 & \cdots & \sigma_\alpha^2 \end{pmatrix},$$

where, the α_0 indicates the initial parameters, which are the measured values. The measurement errors are expressed as σ_i. The λ represents the Lagrange multipliers. The parameters α and β can be obtained to minimize the chi-square value. The degree of freedom (DOF) of this fitting is $4 - b$.

By using the parameters α and their covariance matrix $\boldsymbol{V}$, the χ^2 is minimized with respect to α and λ. The solution is written as,

$$\alpha = \alpha_0 - V_{\alpha_0} D^T \lambda \tag{4.9}$$

$$\lambda = V_D (D\delta\alpha_0 + d)$$

$$V_D = \left(D V_{\alpha_0} D^T\right)^{-1}$$

$$\chi^2 = \lambda^T (D\delta\alpha_0 + d)$$

4.2.3 Calculation of the coplanarity

When a parent hypernucleus decays into three daughter particles, the coplanar of three tracks were examined that they were on the coplanar plane or not in order to emphasize the reaction with or without neutral emission. The coplanarity of three tracks is defined as:

$$c = \left(v_i \times v_j\right) \cdot v_k \tag{4.10}$$

where c is the coplanarity. v_i, v_j, and v_k are the unit vectors for each track respectively.

The value of coplanarity for tracks #7, #8 and #9 was 0.061 ± 0.030. Three tracks from vertex C were coplanar within 2σ.

4.2.4 Calculation of the Ξ^- hyperon binding energy B_{Ξ^-}

The binding energy of the Ξ^- hyperon in the Ξ^--nucleus system is defined as;

$$-B_{\Xi^-} = \sqrt{\left(E_1 + E_2 + \sum_i E_i^0\right)^2 - \left\|p_1 + p_2 + \sum_i p_i^0\right\|^2} - M(\Xi^-) - M({}^{A-1}_{Z+1}\mathrm{X}) \tag{4.11}$$

Where $E_{1,2}$ and $p_{1,2}$ are the total energy and momentum of track #1 and #2. E_i^0 and p_i^0 are the total energy and momentum of the i-th neutral particle. $M(\Xi^-)$ and $M(^{A-1}_{Z+1}\mathrm{X})$ are the masses of Ξ^- and the capturing nucleus.

Figure 4.5 represent the graph of B_{Ξ^-} with the total momentum of all possible decay modes for vertex A. The open circle indicates the decay mode including the estimated mass of single hypernuclei. The magnitude of total momentum of daughter particles was nominated to be zero within 3σ. The value of B_{Ξ^-} was set to be more than zero within 3σ. Although the decay modes with neutral particle/s emissions were kinematically possible, only the red-marked indicates the accepted decay mode by this criterion. This acceptable decay mode was interpreted as following.

$$\Xi^- + {}^{14}\mathrm{N} \rightarrow {}^{10}_{\Lambda}\mathrm{Be}(\#1) + {}^{5}_{\Lambda}\mathrm{He}(\#2). \qquad (4.12)$$

$$\Xi^- + {}^{14}\mathrm{N} \rightarrow {}^{10}_{\Lambda}\mathrm{Be} + {}^{5}_{\Lambda}\mathrm{He}$$

At vertex B, the same criteria of momentum were applied using tracks #3–6. Moreover, the total kinetic energy of the daughter particles must not larger than the Q-value of the reaction process. Since track #1 decayed into four charged particles, the coplanarity was not calculated. The 358 possible decay modes remained within 3σ of energy and momentum conservation. Among these, the decay modes for the case of track #1 being ${}^{10}_{\Lambda}\mathrm{Be}$ were listed in Table 4.6. Many decay modes were accepted because non-mesonic decay has a large Q value. Moreover, at least two neutral particles were likely to be emitted. Hence, the selection with the conservation was not efficient for vertex B. However, the listed thirteen decay modes were all consistent with the result at vertex A.

A different topology may be possible at vertex B. Since the length of track #3 was considerably short, the topology without track #3 was also tested. The coplanarity of tracks #4–6 was obtained to be -0.500 ± 0.034. Some neutral particle emission was expected due to the large coplanarity. The accepted decay modes for the case of track #1 being ${}^{10}_{\Lambda}\mathrm{Be}$ as listed in Table 4.7. From the 48 candidates, the listed four decay modes were consistent with the result at vertex A. In addition, since ^{6}He decays to ^{6}Li + e^- + $\bar{\upsilon}$ with a half-life of 806.7 ms [34], the case of track #4 being ^{6}He was rejected.

In any cases, although the decay mode at vertex B was not determined, track #6 was the most likely to be a proton. At least two neutrons were probably emitted.

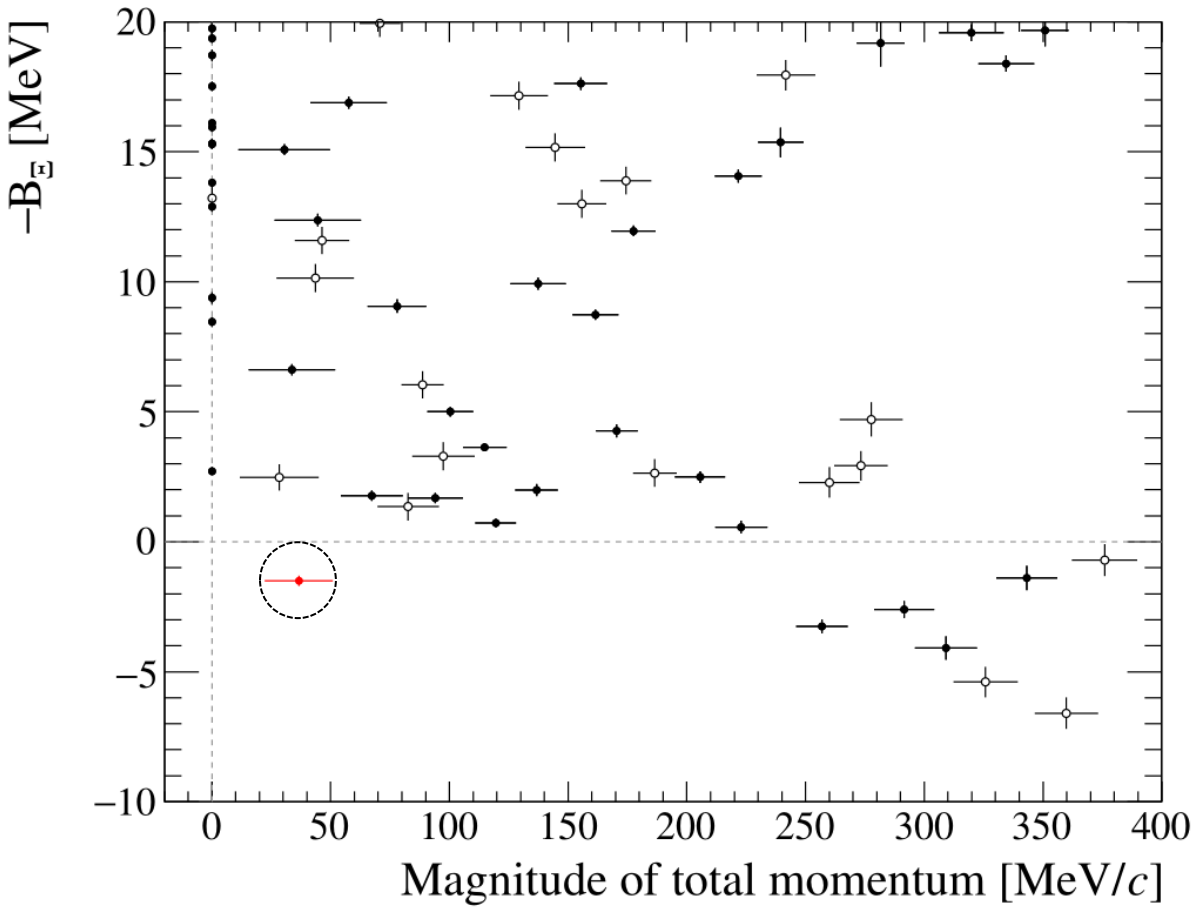

Fig 4.5. Correlation plot of energy versus momentum conservation at vertex A. The open circle indicates the decay mode including the estimated mass of single hypernuclei. The dotted-circle indicates the accepted decay mode.

Table 4.6: Possible decay modes at vertex B for the case of track #1 being ${}^{10}_{\Lambda}$Be.

#3	#4	#5	#6	Missing	Q [MeV]	B_Λ [MeV]
p	d	t	p	$3n$	120.06	< 11.81
p	t	d	p	$3n$	120.06	< 16.36
p	t	t	p	$2n$	126.32	< 12.83
d	p	t	p	$3n$	120.06	< 12.71
d	d	d	p	$3n$	116.03	< 12.89
d	d	t	p	$2n$	122.28	< 10.04
d	t	p	p	$3n$	120.06	< 20.07
d	t	d	p	$2n$	122.28	< 15.27
t	p	d	p	$3n$	120.06	< 17.31
t	p	t	p	$2n$	126.32	< 15.09
t	d	p	p	$3n$	120.06	< 20.15
t	d	d	p	$2n$	122.29	< 15.88
t	t	p	p	$2n$	126.32	< 22.48

Table 4.7 Possible decay modes at vertex B without track #3 for the case of track #1 being ${}^{10}_{\Lambda}$Be.

#4	#5	#6	Missing	Q [MeV]	B_Λ [MeV]
^{3}He	t	p	$3n$	125.55	< 12.13
^{4}He	d	p	$3n$	139.87	< 31.13
^{4}He	t	p	$2n$	146.13	< 24.69
^{6}He	p	p	$2n$	138.63	< 27.68

For vertex C, the consistency with the conservation laws was checked using tracks #7–9. Totally, 263 candidates were accepted within 3σ of energy and momentum conservation. Almost of all were non-mesonic decay modes with multiple neutral particles. The decay modes for the case of track #2 being ${}^{5}_{\Lambda}$He was only one, obtained as the following decay mode,

$$ {}^{5}_{\Lambda}\mathrm{He} \rightarrow {}^{4}\mathrm{He}\ (\#7) + \pi^{-}\ (\#8) + \mathrm{p}\ (\#9) \qquad (4.13) $$

This decay mode was consistent with the σ-stop of the end point of track #8. Furthermore, this mode also had the consistency with the coplanarity of 0.061 ± 0.030. No neutral particle was likely to be emitted from vertex C with 2σ tolerance.

From the above analysis processes, the reaction process of the IBUKI event was interpreted as follows,

$$ \Xi^{-} + {}^{14}\mathrm{N} \rightarrow {}^{10}_{\Lambda}\mathrm{Be}(\#1) + {}^{5}_{\Lambda}\mathrm{He}(\#2), $$

$$ {}^{10}_{\Lambda}\mathrm{Be} \rightarrow (3 \text{ or } 4 \text{ nuclei}, \#3-6) + (2\mathrm{n} \text{ or } 3\mathrm{n}), $$

$$ {}^{5}_{\Lambda}\mathrm{He} \rightarrow {}^{4}\mathrm{He}\ (\#7) + \pi^{-}\ (\#8) + \mathrm{p}\ (\#9). \qquad (4.14) $$

Thus, the formation process of twin single-Λ hypernuclei was uniquely identified as ${}^{10}_{\Lambda}$Be and ${}^{5}_{\Lambda}$He.

In this reaction process at vertex A, the final state was two body in back-to-back direction. If the initial state is at rest, momenta of twin Λ hypernuclei should balance. Since the Ξ^{-} track became a bold and dizzy track at the captured point A, the track range between vertex B and C was measured with the overcomes of the Ξ^{-} captured point. The range from vertex B to C was measured to be 97.1 ± 0.4 μm. Applying the kinematic fitting as described in Section 4.2.2 to the

constraint of the total length, the track ranges of track #1 and 2 were calculated to be 9.40±0.25 μm and 87.72±0.25 μm, respectively, as listed in Table 4.8. The χ^2 value was obtained to be 2.409 with degree of freedom of 2.

Table 4.8 Ranges and emission angles for vertex A with the kinematic fitting.

Vertex	Track	R [MeV]	θ [deg]	ϕ [deg]
A	#1	9.4 ± 0.2	88.6 ± 1.4	302.5 ± 1.2
	#2	87.7 ± 0.2	91.3 ± 1.4	122.5 ± 1.2

The masses of Ξ^- hyperon (1321.71 ± 0.07 MeV/c^2 [32]), ${}^{10}_{\Lambda}$Be (9499.88 ± 0.17 MeV/c^2 [35]), and ${}^{5}_{\Lambda}$He (4839.94 ± 0.02 MeV/c^2 [36]) were taken into account. Thus, B_{Ξ^-} value of 1.27 ± 0.21 MeV represents a bound Ξ^--hypernucleus Ξ^-–^{14}N system. The mass of ${}^{10}_{\Lambda}$Be was evaluated as the average of the 1^- and 2^- states in the ground-state doublet. The energy spacing between these two states is expected to be less than 0.1 MeV. Therefore, the binding energy of the Ξ^- hyperon in the $\Xi^- - {}^{14}$N system, B_{Ξ^-} was obtained to be 1.27 ± 0.21 MeV.

The kinematic fitting was also applied at vertex C. The result is listed in Table 4.9. The χ^2 value was obtained to be 6.622 with degree of freedom of 5. The binding energy of the Λ hyperon in ${}^{5}_{\Lambda}$He, B_{Λ}, was obtained to be 2.77 ± 0.23 MeV, which agrees well with the world average [37].

Table 4.9 Ranges and emission angles for vertex C with the kinematic fitting.

Vertex	Track	R [MeV]	θ [deg]	ϕ [deg]
C	#7	19.1 ± 0.2	87.0 ± 1.0	308.9 ± 0.9
	#8	2146 ± 71	29.5 ± 1.5	236.3 ± 2.2
	#9	2194 ± 28	105.7 ± 1.0	121.6 ± 0.8

The B_{Ξ^-} of 1.27 ± 0.21 MeV indicated that $\Xi^- - {}^{14}\mathrm{N}$ was the bound system. However, the excited state of ${}^{10}_{\Lambda}\mathrm{Be}$ was necessary to be considered. A low-lying excited state at 2.78 ± 0.11 MeV was observed in the measurement of ${}^{10}_{\Lambda}\mathrm{Be}$ spectrum at the missing mass experiment at JLAB [35]. The different of the IBUKI event to the KISO events was because of the small value 1.27 ± 0.21 MeV of B_{Ξ^-}, in which the production of ${}^{10}_{\Lambda}\mathrm{Be}$ at excited state with 2.78 ± 0.11 MeV was excluded. The $\Xi^- - {}^{14}\mathrm{N}$ bound system of the IBUKI event was determined that it was decayed in the ground state of both ${}^{10}_{\Lambda}\mathrm{Be}$ and ${}^{5}_{\Lambda}\mathrm{He}$. The theoretical calculation of B_{Ξ^-} for the $\Xi^- - {}^{14}\mathrm{N}$ system are 5.93 MeV and 1.14 MeV in the nuclear 1*s* (atomic 1*S*) and nuclear 1*p* (atomic 2*P*) states, respectively [29, 37]. Both the Coulomb and nuclear forces are associated in the nuclear 1*p* state and the B_{Ξ^-} were calculated to be 0.39 MeV and 0.75 MeV, respectively. Thus, the B_{Ξ^-}level of in IBUKI event is considered to be the Coulomb-assisted nuclear bound 1*p* state when compared with the theoretical prediction as presented in figure 4.8.

4.3 Analysis of the IRRAWADDY event

The event with three vertexes topology was detected in the downstream of 5th plate of module no. 19 of the emulsion stacks. According to the characteristics of decay topology of this event, it was denoted as twin single-Λ hypernuclear event and named as IRRAWADDY [27, 28].

Figure 4.6 represented the superimposed image and schematic drawing of the IRRAWADDY event. A Ξ^- hyperon came to rest at vertex A, from which three charged particles (tracks #1, #2 and #3) were emitted. Track #1 shows a decay topology at vertex B that is decayed to recoil nuclei (tracks #4 and #5). Track #2 also decayed into two charged particles, tracks #6 and #7 at vertex C. Sine tracks #1 and #2 charged particles have a decay mode each, they are denoted as single-Λ hypernuclei. The hypernuclear event with the production of two single-Λ hypernuclei simultaneously is called twin single-Λ hypernuclear event.

All of the tracks are traced till their stopping points in the emulsion layer. Track #4 have a range in deep direction so that it seems as a very short track while looking from the top side of view. The tracks #3, #4, and #5 stopped in current plate. Thin track #6 going to the upstream direction and stopped in 4th plate with ρ-stop. Another thin track, low ionization track, # 7 going to the downstream direction with long range and stopped in the thin plate, plate no.13th with ρ-stop. Thus, the twin Λ hypernuclei event was observed.

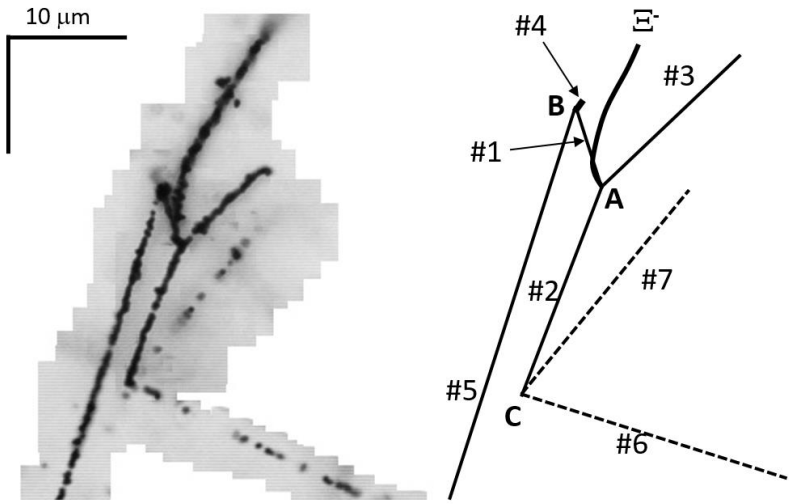

Fig 4.6. Superimposed image (left) and schematic drawing (right) of IBUKI event.

The range measurement of short tracks within a microscopic view was performed with the manner described in Section 3.2. In order to avoid an effect of distortion aberration, the length of track #2 were divided into several segmented data sets. In the case of long tracks out of a microscopic view, the tracks were manually traced to the stopping points. In the case of straight track, the length of segments on the track were measured at intervals of around 50 μm. The range of long tracks was calculated as the length of a polygonal line. Table 4.8 summarizes the measured track ranges and the emission angles of all tracks of the IRRAWADDY event. The angles are expressed by a zenith angle (θ) and an azimuthal angle (ϕ) in respect to the angle perpendicular to the emulsion sheet. For the long tracks, tracks #6 and #7, the ranges going through in a base film were converted to those in the emulsion layer.

Table 4.8: The measured track ranges and emission angles of the IRRAWADDY event.

Vertex	Track	R [μm]	θ[deg]	ϕ[deg]	Comments
A	#1	5.0 ± 0.2	94.7 ± 0.6	291.3 ± 2.6	Single hypernucleus
	#2	12.4 ± 0.2	87.6 ± 0.4	65.3 ± 0.5	Single hypernucleus
	#3	9.8 ± 0.2	94.7 ± 1.7	224.7 ± 2.0	
B	#4	2.3 ± 0.4	168.3 ± 3.5	211.2 ± 16.2	
	#5	189.7 ± 0.6	78.9 ± 1.4	71.9 ± 0.5	
C	#6	2770.5 ± 1.3	116.7 ± 1.4	154.0 ± 0.4	
	#7	8404.2 ± 8.5	27.4 ± 0.8	229.3 ± 1.3	

The same criteria as descripted in section (4.2) of the analysis of IBUKI event was applied. Sine there are three emitted particles at the vertex A, the coplanarity is calculated. The coplanarity of tracks #1, #2 and #3 is -0.049 ± 0.023. Although these tracks are coplanar within 3σ, the conservation of energy and momentum are also necessary to considered. Figure 4.7 shows the graph of B_{Ξ^-} value and the total momentum for the possible decay modes at vertex A. The red circles indicated the accepted decay modes. There are two decay modes in which the magnitude of total momentum was accepted to be zero within 3σ and the value of B_{Ξ^-} was more than zero with 3σ. Table. 4.9 listed these two accepted decay modes with the corresponding B_{Ξ^-} values.

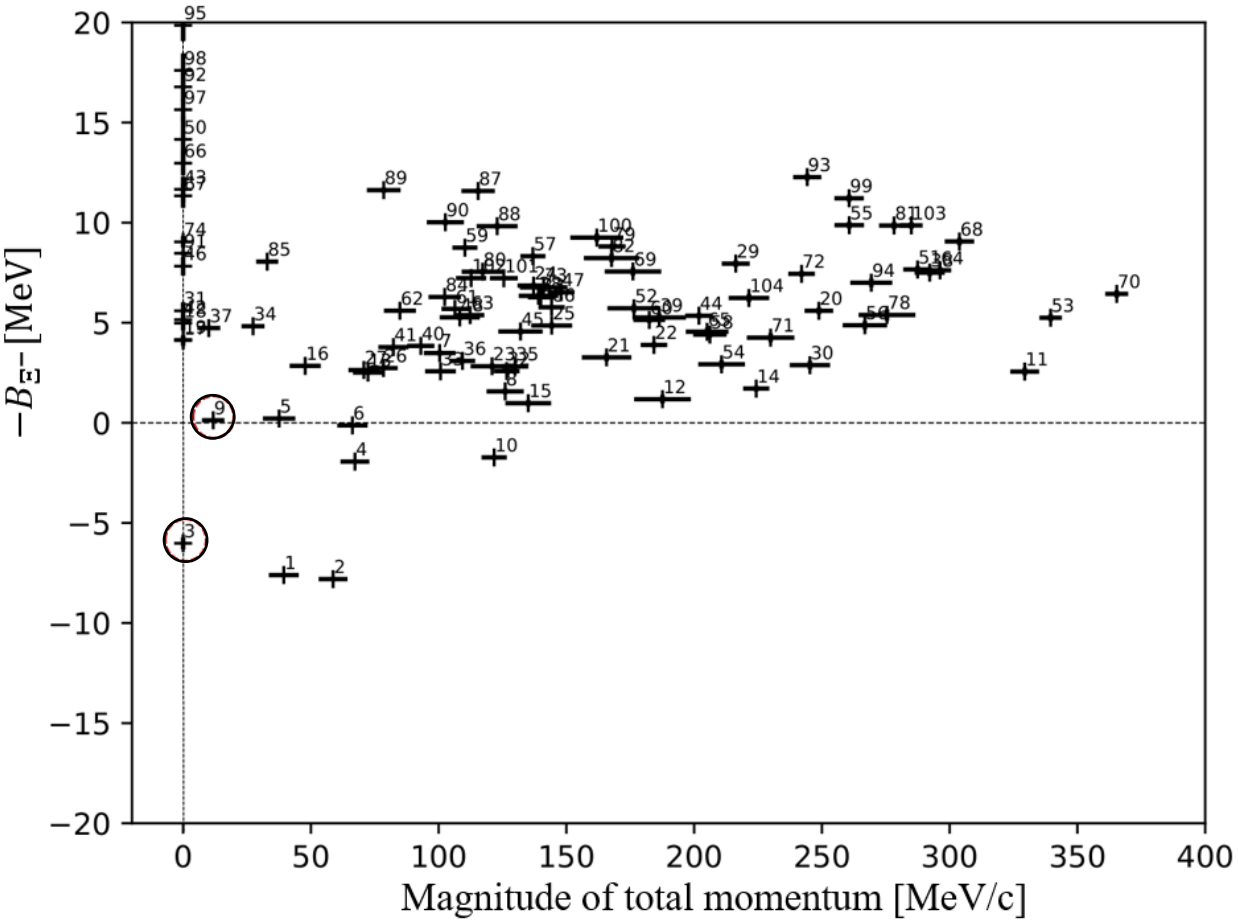

Fig 4.7. Correlation plot of energy versus momentum conservation at vertex A. The circles indicate the accepted decay modes.

Table. 4.9 Possible decay modes at vertex A. The value of B_{Ξ^-} was selected to be more than zero within 3 σ tolerance.

No.	Ξ^- captured		#1	#2	#3	neutral	B_{Ξ^-} [MeV]
1.	$\Xi^- + {}^{12}\mathrm{C}$	→	${}^{4}_{\Lambda}\mathrm{H}$	${}^{4}_{\Lambda}\mathrm{He}$	${}^{4}\mathrm{He}$		-0.128 ± 0.078
2.	$\Xi^- + {}^{14}\mathrm{N}$	→	${}^{5}_{\Lambda}\mathrm{He}$	${}^{4}_{\Lambda}\mathrm{He}$	${}^{4}\mathrm{He}$	n	6.312 ± 0.299

At vertex B and vertex C, there are two decayed daughter charged particles in the direction of none like back-to-back. The momentum will not conserve at these decay points and this missing momentum will get by missing neutral particle/s. The decay modes for the case of track #1 and track #2 being as ${}^{5}_{\Lambda}\mathrm{He}$ are listed in Table 4.10 and Table. 4.11, respectively. Many decay modes were accepted because non-mesonic decay has a large Q value. Moreover, at least two neutral particles were likely to be emitted. Hence, the selection with the conservation was not efficient for vertex B. From the kinematic calculation for track #1 being as ${}^{4}_{\Lambda}\mathrm{H}$ of case No.1 in Table 4.9, there is no possible solution for ${}^{4}_{\Lambda}\mathrm{H}$ decay mode. So that the case No.2 in Table 4.9 of $\Xi^- - {}^{14}\mathrm{N}$ system was determined as the accepted decay mode at vertex A.

Table 4.10: Possible decay modes at vertex B for the case of track #1 being ${}^{5}_{\Lambda}\mathrm{He}$.

SLH (#1)		#4	#5	neutral	Q [MeV]	B_{Λ} [MeV]
${}^{5}_{\Lambda}\mathrm{He}$	→	p	p	3n	144.703	< 137.793
${}^{5}_{\Lambda}\mathrm{He}$	→	p	d	2n	146.927	< 133.755
${}^{5}_{\Lambda}\mathrm{He}$	→	d	p	2n	146.927	< 139.293
${}^{5}_{\Lambda}\mathrm{He}$	→	d	p	π^0 + 2n	11.950	< 4.468
${}^{5}_{\Lambda}\mathrm{He}$	→	t	p	π^0 + n	18.207	< 8.920

Table 4.11: Possible decay modes at vertex B for the case of track #2 being ${}^{5}_{\Lambda}$He.

SLH (#2)		#6	#7	neutral	Q [MeV]	B_{Λ} [MeV]
${}^{5}_{\Lambda}$He	→	p	p	3n	144.703	< 56.686
${}^{5}_{\Lambda}$He	→	p	d	2n	146.927	< 1.833
${}^{5}_{\Lambda}$He	→	d	p	2n	146.927	< 27.795

From the above discussion, the reaction process of IRRAWADDY event was obtained as follows,

$$\Xi^{-} + {}^{14}\mathrm{N} \rightarrow {}^{5}_{\Lambda}\mathrm{He}(\#1) + {}^{5}_{\Lambda}\mathrm{He}(\#3) + {}^{4}\mathrm{He}(\#3) + \mathrm{n}. \qquad (4.15)$$

The single-l hypernuclei, ${}^{5}_{\Lambda}\mathrm{He}(\#1)$ and ${}^{5}_{\Lambda}\mathrm{He}(\#2)$, in equation (4.15) was understand as the decay with multiple of neutral particles emissions as listed in Table 4.10 and Table 4.11. Thus, the formation process of twin single-Λ hypernuclei was uniquely identified. Taking into account of the masses of Ξ^{-} hyperon (1321.71 ± 0.07 MeV/c^2 [32]), and ${}^{5}_{\Lambda}$He (4839.94 ± 0.02 MeV/c^2 [36]), B_{Ξ^-} value of 6.27 ± 0.33 MeV represents a deeply bound Ξ^{-}–^{14}N system. Since ${}^{5}_{\Lambda}$He has no excited state, the value of B_{Ξ^-} could be measured accurately. In comparison with the theoretical prediction, the bound state of IRRAWADDY event is consistent with the nuclear 1*s* state.

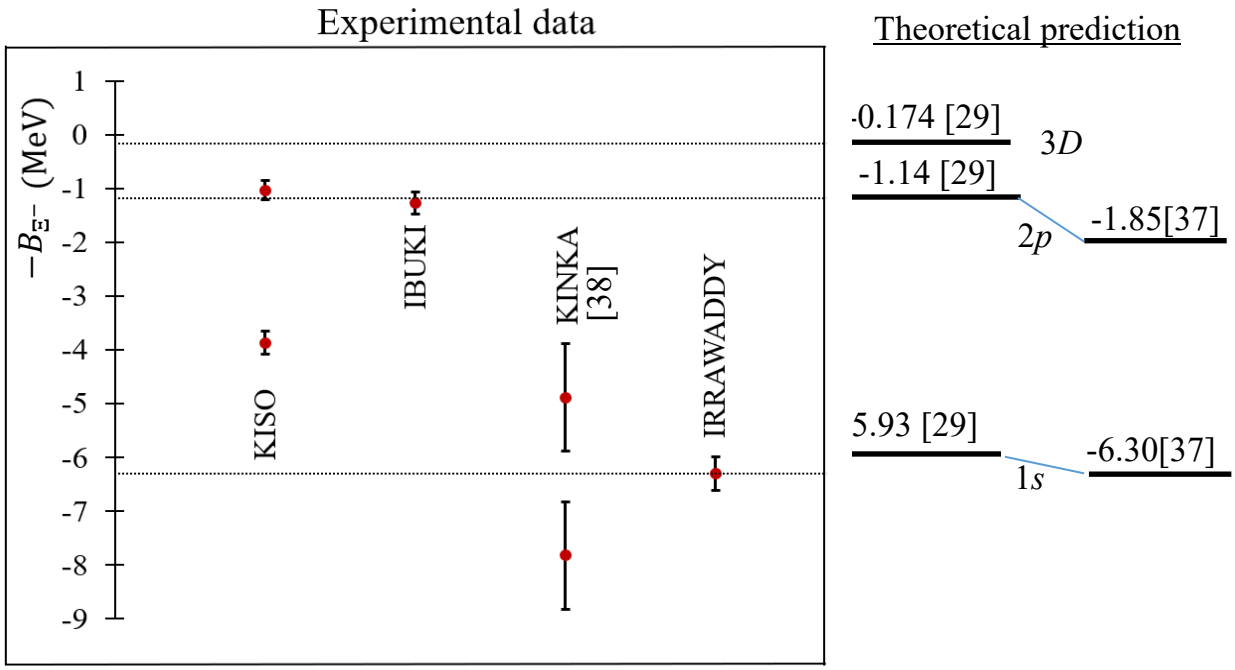

Fig 4.8. The B_{Ξ^-} graph of observed twin single-Λ hypernuclei and the theoretical prediction.

Figure 4.8 represented the comparison of the B_{Ξ^-} values of the experimental data to the theoretical prediction. The KISO and KIKA events analysis showed two possible B_{Ξ^-}values. The shallow states (weakly bound state) of both KISO and IBUKI events are consistent with the calculation for the bound nuclear 1*p* sate. Until now, no experimental dada and theoretical prediction could report about the level-width of the B_{Ξ^-}discretely. According to the theoretical calculation, 3D atomic and nuclear 1p sates were shallow levels. Therefore, we could say that the deeper state (deeply bound state) of KISO event and the two deeper states of KINA event are in the nuclear 1s state, because they are clearly separated from the 1*p* state. The B_{Ξ^-} of IRRAWADDY event was uniquely measured and it was consistent with the nuclear 1*s* state of theoretical prediction. In considering the experimental data and theoretical prediction, the energy levels of Ξ^- of IBUKI and IRRAWADDY events will be the experimental evidences, for the first time, of the nuclear 1*p* and 1*s* states of ${}^{15}_{\Xi}\mathrm{C}$, respectively.

Chapter 5

SUMMARY

An upgraded experiment J-PARC E07 investigated double-Λ hypernuclei to understand the baryon-baryon interaction in SU (3) symmetry. The counter-hybrid emulsion experiments are effective to detect the sequential weak decays specific for the double-Λ hypernuclei. The E07 experiment was performed for a detection of nearly 100 double hypernuclear events with the nuclear emulsion detector. The Ξ^- hyperons were produced via (K^-, K^+) reaction on the diamond target.

A total of 1298 thick type plates and 236 thin type plates were produced using 2.1 tonnes of nuclear emulsion gel from December 2013 to May 2014. The nuclear emulsion of E07 has been exposed to 1.13×10^{11} particles of the K^- beam at J-PARC for two months. By following of Ξ^- tracks for 2 years, 33 DH events were detected. The efficiency of Ξ^- tracks detection in the topmost plate of the emulsion stack is low (~50%) because of the non-uniformity of the gap between the emulsion and detectors. To fulfil the expected number of double hypernuclear events, a new scanning method called "overall scanning" will be applied in the event hunting processes from the 2021 fiscal year and ~ 1000 double hypernuclear event will be detected.

D001 event was likely identified as ${}^{10}_{\Lambda\Lambda}\mathrm{Be}$, via the reaction process of $\Xi^- + {}^{14}\mathrm{N} \rightarrow {}^{10}_{\Lambda\Lambda}\mathrm{Be} + {}^{4}\mathrm{He} + \mathrm{n}$. The $B_{\Lambda\Lambda}$ and $\Delta B_{\Lambda\Lambda}$ values depend on the Ξ^- hyperon binding energy, B_{Ξ^-}. By assuming that the Ξ^- hyperon was captured in the atomic 3*D* state of ^{14}N with the theoretically estimated B_{Ξ^-} value of 0.17 MeV, $B_{\Lambda\Lambda}$ and $\Delta B_{\Lambda\Lambda}$ for ${}^{10}_{\Lambda\Lambda}\mathrm{Be}$ are obtained to be 15.22 ± 2.77 MeV and 1.80 ± 2.77 MeV, respectively.

A newly detected twin single-Λ hypernuclear event, "IBUKI", present a bound Ξ^- hypernucleus, (${}^{15}_{\Xi}\mathrm{C}$), Ξ^-–^{14}N system. The reaction process was clearly identified as $\Xi^- + 14\mathrm{N} \rightarrow {}^{10}_{\Lambda}\mathrm{Be} + {}^{5}_{\Lambda}\mathrm{He}$. Thus, the formation process of twin single-Λ hypernuclei was unique. The binding energy of Ξ^-–^{14}N system was determined to be 1.27±0.21 MeV by applying the kinematic fitting.

By considering the experimental data and the theoretical calculations, the energy level of Ξ^- is likely the Coulomb-assisted nuclear 1*p* state.

Another newly detected twin single-Λ hypernuclear event, IRRAWADDY, was uniquely identified as the reaction process of $\Xi^- + 14\mathrm{N} \rightarrow {}^{5}_{\Lambda}\mathrm{He}(\#1) + {}^{5}_{\Lambda}\mathrm{He}(\#3) + {}^{4}\mathrm{He}(\#3) + \mathrm{n}$. The binding energy of Ξ^-–^{14}N system was measured to be 6.3±0.3 MeV. The value of B_{Ξ^-} represents a very deeply bound Ξ^-–^{14}N system. This is the first observed in the world experimentally. By

considering the experimental data and the theoretical calculations, the energy level of Ξ^- is likely the nuclear 1*s* state captured.

Acknowledgement

First and foremost, I would like to offer my special thanks to my supervisor, Senior Professor Dr. Kazuma NAKAZAWA for his invaluable supervision and continuous support during my study for Ph. D degree. Without his supervision and proper guidance, I could not have done my research.

The next person whom I would like to extend my sincere thanks to Professor Kaoru HOSHINO and Professor Kazuroni ITONAGA for their insightful comments and suggestions in laboratory seminars.

Besides, I would like to express my thanks to Dr. Masahiro YOSHIMOTO for his advices and technical support, hardware and software throughout my research, and my thanks go to Dr. Junya YOSHIDA, Dr. Shuhei HAYAKAWA and Dr. Hiroyuki EKAWA for their help, patience discussions and advices through group meetings and personal discussions.

I would like to give my thanks to Mr. Ayumi KASAGI and Ms. Phyo Myat LIN who are first year Ph. D students from Gifu University for their help and support when I am carrying my research work. I would also like to give my thanks to all students who are attending and presenting their work at weekly laboratory seminar.

I would like to express my appreciates to the members of AGP program from the Graduate school of engineering, Gifu University for giving a chance to study and providing financial support for my study life in Japan. I would also like to express my appreciate to the scholarship foundations, Heiwa Nakajima and IUCHI for one-year financial support.

Finally, I would like to express my sincere gratitude to my family and friends for their encouragement and support throughout my studies.

References

[1] O. Hashimoto and H. Tamura, Prog. Part. Nucl. Phys. **57**, 564 (2006).

[2] H. Noumi et al., Phys. Rev. Lett. **89**, 072301 (2002).

[3] M. Tanabashi et al. (Particle Data Group), Phys. Rev. D **98**, 030001 (2018).

[4] M. Danysz et al., Nuclear Physics **49**, 121 (1963).

[5] S. Aoki et al., Nucl. Phys. A **828**, 191 (2009).

[6] S. Aoki et al., Prog. Theor. Phys. **85** 1287 (1991).

[7] H. Takahashi et al., Phys. Rev. Lett. **87**, 212502 (2001).

[8] J. K. Ahn et al., Phys. Rev. C **88**, 014003 (2013).

[9] H. Ekawa et al., Prog. Theor. Exp. Phys. **2019** 021D02 (2019).

[10] E. Hiyama et al., Phys. Rev. C **66**, 024007 (2002).

[11] A. Gal and D.J. Millener, Phy. Let. B **701**, 342 (2011).

[12] Wen-Ying Li, Ji-Wei Cui, and Xian-Rong Zhou, Phys. Rev. C **97**, 034302 (2018).

[13] Yoshiko Kanada-En'yo, Phys. Rev. C **97**, 034324 (2018).

[14] K. Nakazawa et al., Prog. Theor. Exp. Phys. **2015**, 033D02 (2015).

[15] E. Hiyama and K. Nakazawa, Annu. Rev. Nucl. Part. Sci. **68**, 131 (2018).

[16] K. Nakazawa, K. Imai, and H. Tamura, et al., J-PARC P07 proposal (2006)

[17] H. Takahashi, Ph.D Thesis, Phys Department, Kyoto University (2003).

[18] H. Ito, M.Sc Thesis, Education Faculty, Gifu University (2005).

[19] H. Ekawa, Ph.D Thesis, Phys Department, Kyoto University (2019).

[20] M. K. Soe, et ai, Nucl. Instrum. Meth. Phys. Res. A, **848**, 66 (2017).

[21] W. H. Barkas, P. H. Parrett, P. Cüer and H. H. Heckman, Nuovo Cimento, **8**, 185, (1958).

[22] H. H. Heckman et al., Phys. Rev. **117**, 544, (1960).

[23] J. Yoshida et al., Nucl. Instrum. Methods Phys. Res. Sect. A **847**, 86-92 (2017).

[24] S. Kinbara et al., Prog. Theor. Exp. Phys. **2019**, 011H01 (2019).

[25] A. N. L. Nyaw, et al., Bull. Soc. Photogr. Imag. Japan. Vol. **30,** No. 2 (2020).

[26] S. Hayakawa, et al., Phys. Rev. Lett. **126**, 062501 (2021).

[27] IRRAWADDY is name of the biggest and longest river in Myanmar flowing from north to south. Photo available; https://en.wikipedia.org/wiki/Irrawaddy_River.

[28] M. Yoshimoto, et al., (arXiv:2103.08793v1 [nucl-ex] 16 Mar 2021).

[29] M. Yamaguchi, K. Tominaga, Y. Yamamoto, and T. Ueda, Prog. Theor. Phys. **105**, 627 (2001).

[30] D. H. Davis, Contemporary Physics, **27:2**, 91 (1986).

[31] M. Tanabashi et al. (Particle Data Group), Phys. Rev. D **98**, 030001 (2018).

[32] Particle data group, Phys. Lett. B 667, 1061 (2008).

[33] P. Avery, Applied Fitting Theory I: General Least Squares Theory, CLEO Note CBX, 91–72, (1991).

[34] D. R. Tilley et al., Nucl. Phys. A **708**, 3 (2002).

[35] T. Gogami et al., Phys. Rev. C 93, 034314 (2016).

[36] M. Juric et al., Nucl. Phys. B 52, 1 (1973).

[37] M. M. Nagels, Th.A Rijken, Y. Yamamoto, arXiv:1504.02634v1 (2015).

[38] Y. Nagase, Master Thesis, Faculty of Education, Gifu University.